공학박사 학위논문

Fabrication and characterization of high-performance quantum-dot light-emitting diodes

고성능 양자점 발광다이오드의 제작 및 소자 특성

2012 년 8 월

서울대학교 대학원

공과대학 전기컴퓨터공학부

조 현 덕

Fabrication and characterization of high-performance quantum-dot light-emitting diodes

지도교수 이 창 희

이 논문을 공학박사 학위논문으로 제출함

2012 년 8 월

서울대학교 대학원

공과대학 전기컴퓨터공학부

조 현 덕

조현덕의 박사 학위논문을 인준함

2012 년 7 월

위 원 장 _____ (인)

부위원장 _____ (인)

위 원 _____ (인)

위 원 _____ (인)

위 원 _____ (인)

Abstract

Fabrication and characterization of high-performance quantum-dot light-emitting diodes

Hyunduck Cho

School of Electrical Engineering and Computer Science

The Graduate School

Seoul National University

Recently, the interest on colloidal quantum-dot light-emitting diodes (QLEDs) for lighting and display applications have been growing due to the novel material properties such as high color purity, ease of color control and process simplicity. Since the first report in 1994 by Alivisatos group, the device performances of QLEDs have been developed substantially with multilateral efforts on material synthesis, electrophysical analysis, device design and fabrication processes. However, their performance needs to be further improved, in order to be comparable with other matured technologies such as organic light-emitting diodes (OLEDs).

In this thesis, we have investigated the device performance of QLEDs fabricated by using soft-contact transplanting method. Soft-contact transplanted QLEDs showed comparable performances to conventional spin-

coated QLEDs. We also studied the patternability of QDs on various vacuum-deposited hole transporting layers (HTLs). When the work of adhesion between the hole transporting material (HTM) and QDs were higher, the QD patterns were transferred better. Since the QD transplanting method enables us to deposit the QD layer without damaging the underlying organic HTM, we can fabricate highly efficient QLEDs by transplanting the QDs on HTLs with high highest occupied molecular orbital (HOMO) levels which are beneficial to inject holes to the valence band of QDs.

In addition, we developed highly transparent and flexible QLEDs (TFQLEDs) by laminating *p*-doped graphene electrode as an anode in the inverted structure where the ITO acts as a cathode with ZnO nanoparticles as an electron injection layer. The red, green and blue TFQLEDs showed excellent transparency and high efficiency. Due to higher transmittance of graphene electrode, graphene side emission was larger than ITO side emission in the green–blue region. Angular dependent electroluminescence characteristics almost followed the Lambertian profile. Finally, we can successfully developed red, green and blue TFQLEDs using graphene electrodes for both anode and cathode by replacing ITO electrode with a UV-ozone treated graphene electrode. We think that the fabrication methods and device structures developed in this thesis are helpful for realizing various transparent and flexible optoelectronic devices.

Keywords: colloidal quantum dot, light-emitting diodes, graphene electrodes, QD transplanting method

Student Number: 2006-23202

Contents

List of Tables

List of Figures

Chapter 1. Introduction

1.1 Quantum-Dot Light-Emitting Diodes

Colloidal quantum dots (QDs) have advantages in optical and electrical properties in terms of high photoluminescence (PL) quantum yields, broad absorption area, narrow emission spectra, high colloidal and electrical stability, and processability. Therefore, quantum-dot light-emitting diodes (QLEDs) using these colloidal QDs as emitters have great advantages such as high color purity, solution-based easy process. Although organic light-emitting diodes (OLEDs) have various advantages, the emission spectrum of each color is quite broad (FWHM > 40 nm) which limits the color express-range. Compared to OLEDs, QLEDs exhibit very low spectral bandwidths (FWHM < 30 nm) so that it can show extremely high color-purity in each color. In Figure 1.1, typical electroluminescence (EL) spectra of OLEDs and QLEDs for red, green and blue colors were compared. Red, green and blue EL spectra of OLEDs were taken from the phosphorescent devices using emission layers of bis(1-phenylisoquinolinato) iridium(III) (acetylacetonate) ($(piq)_2Ir(acac)$)- and fac-tris(2-phenylpyridine) iridium(III) ($Ir(ppy)_3$)-doped 4,4'-N,N'-dicarbazole-biphenyl (CBP) layers and iridium(III) bis(4,6-(difluorophenyl) pyridinato-N,C2') picolinate (Firpic)-doped N,N'-dicarbazolyl-3,5-benzene (mCP) layer. Owing to the advantages, QDs are considered as the most

promising material for displays and backlight unit for liquid crystal displays (LCDs).

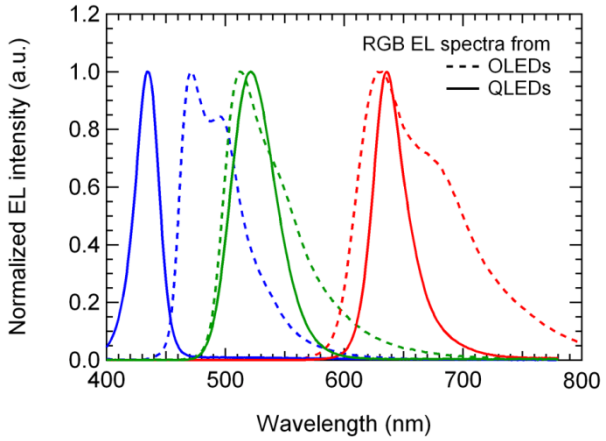

Figure 1.1 Comparison of red, green and blue electroluminescence spectra with (dashed lines) OLEDs and (solid lines) QLEDs.

The first QLED was demonstrated by V. L. Colvin *et al.* [1]. The device was comprised of *p*-paraphenylene vinylene (PPV) / CdSe bilayer between ITO anode and Mg cathode. The device showed a maximum brightness of 100 cd m^{-2} and a low external quantum efficiency of 0.001–0.01%. In addition, the most of electroluminescence was originating from both PPV and QDs, which caused low efficiency and low color purity. Then, S. Coe *et al.* reported the QLED structure which isolated the luminescence processes from charge conduction [2]. After a few decades since first QLED demonstration, great progress (more than 100-folds in terms of brightness, efficiency and color-purity) has been achieved. As shown in Figure 1.2, the external quantum efficiency (EQE) of QLEDs has been increased rapidly for 2 decades.

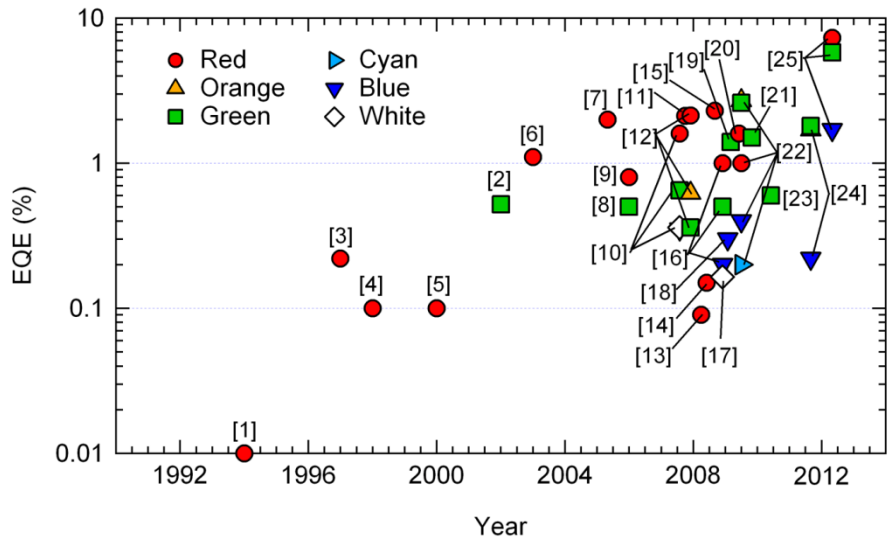

Figure 1.2 Progress in external quantum efficiency (EQE) of QLEDs. The EQE values were categorized into six colors of red (770–600 nm), orange (600–570 nm), green (570–500 nm), cyan (500–480 nm), blue (480–430 nm) and white.

After that, the research on QLED had been reported continuously [10,14,27,28], however, the devices had problems in emitting own spectra of QDs and low efficiency. Due to a large energy barrier between quantum-dot emitting material (the valence band edge is ~7 eV) and organic hole transporting material (HTM) (the highest occupied molecular orbital (HOMO) energy level is 5–6 eV), hole injection from organic layer into QDs is not easy, which results in low efficiency as well as parasitic emission from adjacent organic layers [25]. QD deposition on an organic hole transporting layer (HTL) was also issued. Because of colloidal QDs dissolved in organic solvent which also dissolving organic HTMs, in order to deposit bilayers of HTM and QDs

with solution-based process, phase separation technique was typically used [2,6,7]. When the mixture solution of organic HTM and QDs was deposited on the substrate, they aggregated separately forming bilayer structure. However, phase-separation of QDs does not make perfect bilayer (i.e., QDs aggregated to not only top side, but also bottom side of hole transporting layer), which results in low efficiency and parasitic emission by exciton formation in organic layers. Since that, Q. Sun *et al.* fabricated the stacked structure using robust and resistive polymer HTL to QD deposition [12]. Those QLEDs using a similar structure of organic light-emitting diodes showed high performance. The devices showed red, yellow, orange and green colors with the maximum brightness of 9,000, 3,200, 4,470 and 3,700 cd m^{-2}, respectively. For the red device, a high efficiency of 2.8 cd A^{-1} was achieved with enhanced stability (half luminance lifetime of ~300 h). After that, a lot of research results on QLEDs have been reported with various methods such as inkjet printing [29], contact printing [15,16,20,22,24,28], or metal oxide inorganic layers [13].

Among several deposition techniques, transfer methods were successfully employed in fabricating efficient QLEDs. The transfer processes used in QLED fabrication had slight differences among research groups. However, the advantages of those methods are summed up in the following two points: solvent-free QD deposition and ability to pattern QL layers. Using transfer method, P. O. Anikeeva *et al.* demonstrated QLEDs emitting emission colors over the entire visible spectrum from blue (EL_{max} at 460 nm) to red (EL_{max} at 650 nm) [10]. Recently, the first active matrix display device

using transfer-printed QDs on hafnium-indium-zinc oxide (HIZO) thin-film transistor backplane by Samsung Advanced Institute of Technology (SAIT) [26]. Cross-linkable hole transporting material (poly[9,9-dioctylfluorenyl-2,7-diyl)-co-(4,4′-(*N*-(4-sec-butylphenyl))diphenylamine)]; TFB) and sol-gel TiO_2 as an electron transporting material were adopted to fabricate the device with solution based process. The transfer-printed red, green and blue QD-based LEDs having EL peaks at 615, 530 and 480 nm showed high luminance values of 16,380, 6,425 and 423 cd m^{-2}, respectively. For the printed red QLED, power efficiency of 4.25 lm W^{-1} was achieved. Turn-on voltage of the device was also as low as 1.7 V with red emission (peak at 615 nm in PL) [20]. Display device was 4-inch in size with a 320 × 240 pixel array with the active matrix drive was demonstrated as shown in Figure 1.3, which represents that QLED display will be realized before long.

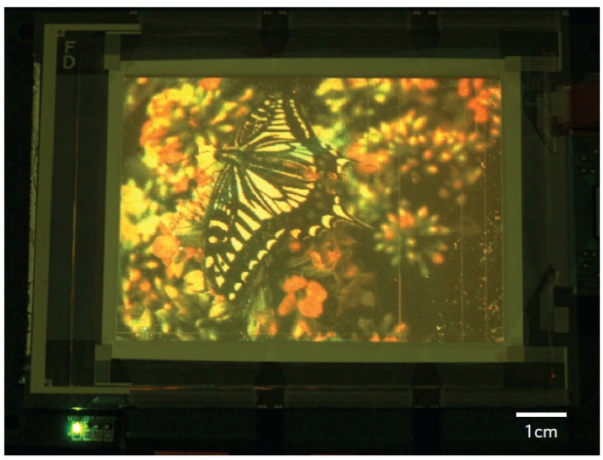

Figure 1.3 The image of a 4-inch full-color QD display using a HIZO TFT backplane with a 320×240 pixel array [26]. (The image is taken from ref. [26].)

1.2 Flexible and Transparent electrodes for light-emitting diodes

Transparent and flexible electronics have attracted a great deal of interest in recent years since they offer advantages for a wide range of applications such as displays, lighting, solar cells, and sensors [30]. In particular, high transparency is an important requirement for realizing informational displays on windshields or eyeglasses. Indium tin oxide (ITO) has been most commonly used as a transparent electrode due to their high conductivity and reasonable transparency [31]. The first transparent OLED employed ITO as the transparent electrode and then a thin Mg:Ag layer deposited directly on the organic active layer followed by deposition of a thicker layer of ITO as the transparent anode [32]. The EQE was low as 0.75% and the average transmittance was 57.7% in the visible range of 400–800 nm. However, when applying ITO as a top electrode, such devices were obliged to suffer from damaging underlying organic layers during sputter deposition [32–34]. In addition, ITO will undergo an increase in cost due to the depletion of world reserves of indium [35]. As the alternative way to protect the active layer, depositing ITO at a low rate and inserting a buffer layer between the active layer and final ITO electrode were used [36,37]. These devices exhibited better transparency, however, they still suffer from not only low transparency in the blue region due to absorption from ITO but also microcavity effects due to the buffer layer or relatively high reflectivity of ITO leading to different

emission spectra from each side of the device. Although depositing thin metal film using thermal evaporation can avoid this damage problem, it also has drawbacks of limited transparency, significant reflectance leading to microcavity effects [38,39]. Also, carbon nanotube networks were applied to an OLED as a transparent electrode [40]. However, the sheet resistance of a carbon nanotube film is high, therefore thick layers must be used to increase conductivity and achieve reasonable device performance, leading to significantly reduced transparency.

Graphene, the 2-dimensional analog of a carbon nanotube, has recently emerged as a potential transparent electrode for replacement of ITO. The transparency of graphene depends linearly on the number of layers. Only a few layers are needed to make a conductive transparent electrode and ITO-comparable sheet resistance of ~30 $\Omega\ \square^{-1}$ was achieved at ~90% transparency that remained unchanged upon bending [41,42]. Furthermore, graphene sheets show very low reflectivity [43]. Initially, graphene sheets were obtained by mechanical exfoliation of graphite. While the quality of graphene sheets obtained by mechanical exfoliation is very good, it is not possible to form reproducible, patternable and large area sheets via this method. Other methods for obtaining graphene sheets include reduction of solution-processed graphene oxide [44]. Such graphene sheets have been successfully implemented in organic solar cell and OLED configurations [45,46]. However, the sheet resistance in solution-processed graphene is significantly higher than in exfoliated graphene leading to relatively poor device performance. Recently, S. Bae *et al.* reported the deposition of graphene sheets via chemical vapor

deposition (CVD) for large area and also demonstrated graphene-based touch-screen panel [42] (see Figure 1.4). The CVD-grown graphene sheets exhibited similar conductivity and transparency compared to that of exfoliated graphene. High-quality large-scale graphene sheets can be easily produced by a roll-to-roll processing, patterned and doped increasing out of plane conductivity.

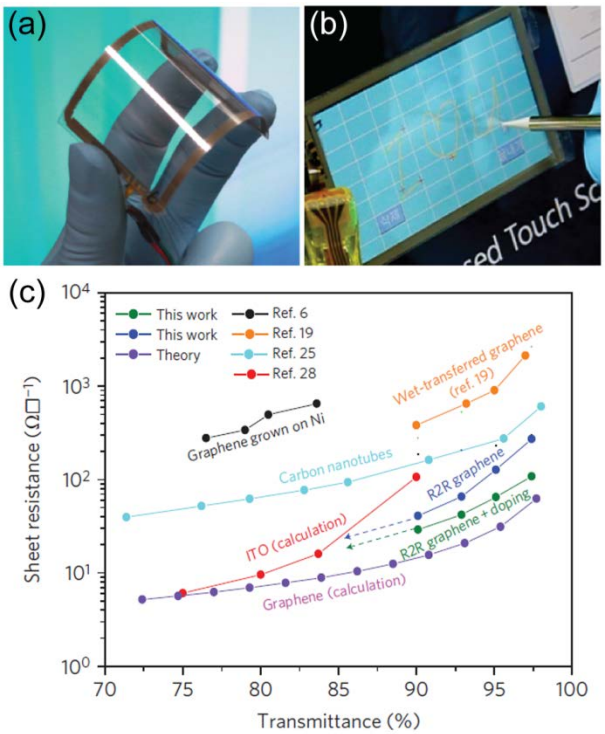

Figure 1.4 (a) The graphene-based touch panel assemble with high flexibility and (b) the demonstration of the 3.1-inch touch panel. (c) The sheet resistance–transmittance characteristics of various transparent electrodes. ((a,b) The images and (c) the graph are taken from ref. [42].)

1.3 Outline of Thesis

This thesis is composed of five chapters including **Introductions** and **Conclusion**. As an introductory part, **Chapter 1** provides the previous studies of quantum-dot light-emitting diodes and transparent flexible electrodes for light-emitting diodes. In **Chapter 2**, preparation methods of highly luminescent red, green and blue quantum dots, ZnO nanoparticles and transparent graphene films are described in detail. Also, the fabrication and characterization methods for the QLED devices are summarized in this chapter. Soft-contact transplanted QD layers were systematically studied by characterizing the film properties and QLEDs using those layers in **Chapter 3**. Red, green and blue QLEDs using transplanting method showed compatible performances with those using spin-coating method. The solvent-free and pressure-free properties of transplanting method enable QDs to be transferred on vacuum-deposited organic materials. Transplanted QD patterns on the various organic hole transporting layers showed different patternability. Higher QLED performances were obtained by lowering hole injection barrier with vacuum-deposited hole transporting layer. Finally, the demonstration of transparent and flexible QLEDs with graphene electrodes is provided in **Chapter 4**. In order to use graphene electrodes in a QLED, optimization of efficient carrier injection is needed. To inject holes and electrons from graphene electrode, *p*-doping and UV-ozone treatment were adopted, respectively. In an inverted structure, transparent top anodes were formed by laminating graphene-attached PDMS. Transparent and flexible QLEDs using

graphene electrodes showed good device performances in terms of brightness, efficiency and turn-off state transparency.

Chapter 2. Experimental Methods

2.1 Preparation of Quantum Dots and ZnO Nanoparticles

The colloidal QDs of CdSe/CdS/ZnS, CdSe@ZnS and $Cd_{1-x}Zn_xS$@ZnS were prepared as the red, green and blue emitters, respectively [47]. These QDs were synthesized in the method of the previous reports [48–50]. Schematics of red, green and blue luminescent QDs are shown in Figure 2.1.

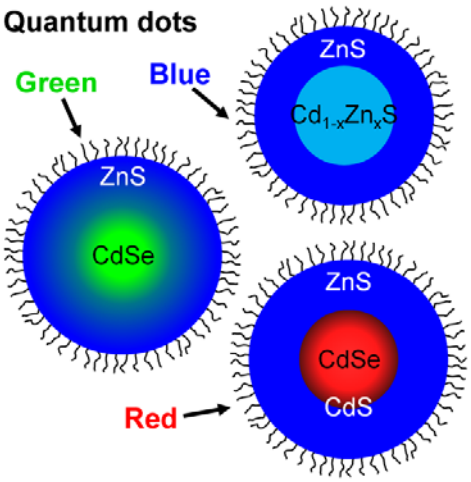

Figure 2.1 Compositional structure of red, green and blue QDs used in this thesis. The surfactant-capped core/shell nanostructure was used with different size and composition.

2.1.1 Synthesis of green- or red-color emitting $Cd_{1-x}Zn_xSe_{1-y}S_y$ quantum dots with chemical composition gradient

As a synthetic procedure, 0.4 mM of cadmium oxide (CdO, 99.99 %), 4 mM of zinc acetate ($Zn(acet)_2$, 99.9 %), 17.6 mM of oleic acid (OA, 90 %), and 20 mL of 1-octadecne (1-ODE, 90 %) were placed in a 100 mL round flask. The mixture was heated to 150 °C, degassed under 100 mTorr pressure for 20 minutes, filled with N_2 gas, and further heated to 310 °C to form a clear solution of $Cd(OA)_2$ and $Zn(OA)_2$. At this temperature, 0.4 mM of Se powder and 4 mM of S powder both dissolved in 3 mL of trioctylphosphine (TOP, 90 %) were quickly injected into the reaction flask. After the injection, the temperature of the reaction flask was set to 300 °C for promoting the growth of QDs, and it was then cooled to room temperature to stop the growth. QDs were purified by adding 20 mL of chloroform and an excess amount of acetone (3 times); they were then redispersed in chloroform or n-hexane. In order to tune the optical properties of QDs, we changed the ratios of Cd to Zn and Se to S with the total concentrations of the Cd-Zn pair and Se-S pair fixed at 4.4 mM, while we maintained all the other parameters such as the amounts of OA, ODE, or TOP, reaction temperature, and reaction time constant [47,48].

2.1.2 Synthesis of blue-color emitting $Cd_{1-x}Zn_xS$@ZnS quantum dots

As a synthetic procedure, 1 mM of CdO, 10 mM of $Zn(acet)_2$, 7 mM of OA were placed in a 100 mL round flask. The mixture was heated to 150 °C, degassed under 100 mTorr pressure for 20 minutes, filled with N_2 gas, added with 15 ml of 1-ODE and further heated to 300 °C to form a clear solution of $Cd(OA)_2$ and $Zn(OA)_2$. At this temperature, 2 mM of S powder dissolved in 3 mL of 1-ODE were quickly injected into the reaction flask. After the first injection of S precursors, the temperature of the reaction flask was elevated to 310 °C for further growth of $Cd_{1-x}Zn_xS$ cores. After the elapse of 8 min of reaction, 8 mM of S powder dissolved in tributylphosphine (TBP, 90 %) were introduced into the reactor to overcoat existing $Cd_{1-x}Zn_xS$ cores with ZnS shells without any purification steps. Aliquots of QDs were taken during the reaction to analyze the development of QDs. After the reaction was completed, the temperature was cooled down to room temperature. QDs were extracted and purified by adding 20 ml of chloroform and an excess amount of acetone (done twice); then they were redispersed in chloroform or hexane for further characterization. In order to adjust the optical properties of QDs, the amount of S precursors in the first injection was varied maintaining the other entire parameters constant.

2.1.3 Preparation of ZnO nanoparticles

ZnO nanoparticles were prepared [47] modifying the method reported by C. Pacholski *et al.* [51]. At first, 1.23 g of $Zn(Ac)_2 \cdot 2H_2O$ was dissolved in 55 ml of methanol at room temperature. Then, 25 ml of a methanol solution containing 0.48 g of KOH was added dropwise at 60 ºC with magnetic stirring. The reaction mixture was kept at 60 ºC with magnetic stirring for 2 h under N2 flow. The product appeared as white precipitate. After collecting by centrifugation, this white precipitate was washed with methanol. Finally, the precipitate could be redispersed in n-butanol. For determining the ZnO concentration, a known amount of the colloidal solution was dried and the residual powder was weighed.

2.2 Preparation of Transparent Graphene Electrodes

Transparent graphene electrodes are prepared with the previously reported methods [41,42]. A 4-layer graphene film was transferred to polyethylene terephthalate (PET) or polyether sulfone (PES) substrate.

For PET / graphene samples, the roll-based transfer method was used as shown in Figure 2.2. First, monolayer graphene film was synthesized on a roll of copper foil in the CVD system having an 8-inch-wide tubular quartz reactor. In order to increase the grain size of the inserted copper foil, it was heated to 1000 ˚C with flowing 8 s.c.c.m. H_2 at 90 mTorr and annealed for 30 min. Then, for graphene growth, gas mixture of CH_4 (24 s.c.c.m.) and H_2 (8 s.c.c.m.) were flowed at 460 mTorr for 30 min and the samples were rapidly cooled down to room temperature at a rate of 10 ˚C s^{-1} with the flow of H_2 at 90 mTorr. A synthesized monolayer graphene film was attached to a thermal release tape at a pressure of 0.2 MPa. Second, the copper foil was etched in a plastic bath with copper etchant and rinsed with deionized (DI) water. Finally, target substrate and graphene-attached thermal release tape were inserted together in the roller and heated with a temperature of 90–120 ˚C. The graphene film was transferred to target PET substrate and those transfer procedures were repeated four times, resulting in a PET / (4-layer) graphene sample. For PES / graphene samples, a floating-catching method was used. A PES substrate (STH200) was purchased from i-components. As described above, a monolayer graphene was synthesized on a copper foil and the foil was etched in the etchant-filled bath without attaching the thermal release tape.

The graphene film was floated in the bath and caught by PES substrate. The monolayer graphene on PES substrate was dried at 70 ˚C. Repeating those steps four times resulted in the PES / (4-layer) graphene.

The multilayer graphene film on plastic substrate was patterned by a photolithography process.

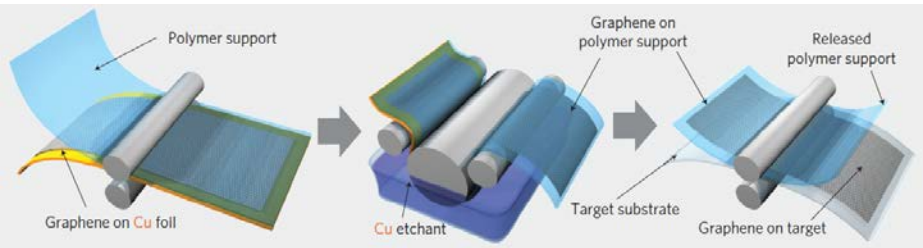

Figure 2.2 Schematic of the roll-to-roll transfer process of graphene films from a copper foil to a plastic substrate. (The schematic is taken from ref. [42])

2.3 Fabrication and Characterization Methods

2.3.1 Device fabrication

All devices used in this thesis have slightly different structure in each chapter to obtain optimized performances. Specified device structures, process or chemical materials are described in each chapter. Typical device fabrication methods are as follows: The patterned indium-tin oxide (ITO) glass substrates were cleaned in ultrasonic bath (Branson 5510) with isopropyl alcohol (IPA), acetone, methanol and deionized (DI) water. For an ITO plastic substrate, an ITO-deposited PES substrate (STI200, i-components) was patterned with a photolithographical method and rinsed with IPA. The cleaned substrates were dried in ambient oven at 120 °C for more than 30 minutes. For the standard structure, glass / ITO substrates were treated with ultraviolet-ozone cleaner (UVO-42) to remove the surface hydrocarbon contamination and increase the work function of ITO when we employed poly(3,4-ethylenedioxythiophene):poly(styrenesulfonate) (PEDOT:PSS, CLEVIOS™ P VP AI 4083, H. C. Starck) as a hole injecting layer (HIL). Deposited PEDOT:PSS film was dried in vacuum oven at 120 °C for 30 min. For the inverted structure, a glass / ITO (15 Ω $\square^{-1}$) or PES / ITO (100 Ω $\square^{-1}$) substrate was not UV-ozone treated and on top of that, ZnO layers were deposited by spin-coating at a speed of 2,000 rpm for 60 sec, followed by drying in N_2 oven at a temperature of 90 °C. QDs were deposited by spin-

coating at a speed of 4,000 rpm for 30 sec, followed by drying in N_2 oven at a temperature of 70 °C. The vacuum deposition of thin films was performed by thermal evaporation under a base pressure of 1–5 × 10^{-6} Torr at a rate of 1-2 Å s^{-1} for organic semiconducting materials, 0.05–0.08 Å s^{-1} for LiF (electron injecting material), 0.1–0.5 Å s^{-1} for MoO_3 (hole injecting material) and 3–6 Å s^{-1} for Al (metal cathode), respectively. The evaporation speed was monitored with a quartz-oscillator thickness monitor. The emitting area is 1.4 × 1.4 mm^2 which is defined by the crossing overlap of anode and cathode.

2.3.2 Preparation of hard/soft molds for QD patterning

For a soft mold, we used poly(dimethylsiloxane) (PDMS, Sylgard 184) which was purchased from Dow Corning and for a relatively hard mold, UV-curable poly(urethane acrylate) (PUA, 311RM) which was purchased from Minuta Tech. A 1-μm-depth Si master mold has line-and-space stripe patterns with various widths of 2, 4, 6, 8 and 10 μm and dot patterns with a diameter of 2 μm. Patterned PUA stamp was prepared by the following steps. PUA solution was added dropwise onto the Si master. The PET film was placed on the Si master. For curing PUA, UV light was irradiated through the PET film for 4 min. Then, the PET / PUA mold was detached from the Si master. To cure firmly PET / PUA mold, PET / PUA mold was turned over and UV-cured for 4 min again. Patterned PDMS stamp was prepared by curing the mixture of Sylgard 184 A and B (with a volume ratio of 10:1) on the Si master or PUA

mold at 60 °C for 1 h in N_2 oven and was surface modified with UV-ozone treatment for 4 min to enhance the adhesion between the PDMS stamp and QDs. The schematic diagram of mold preparation is shown in Figure 2.3.

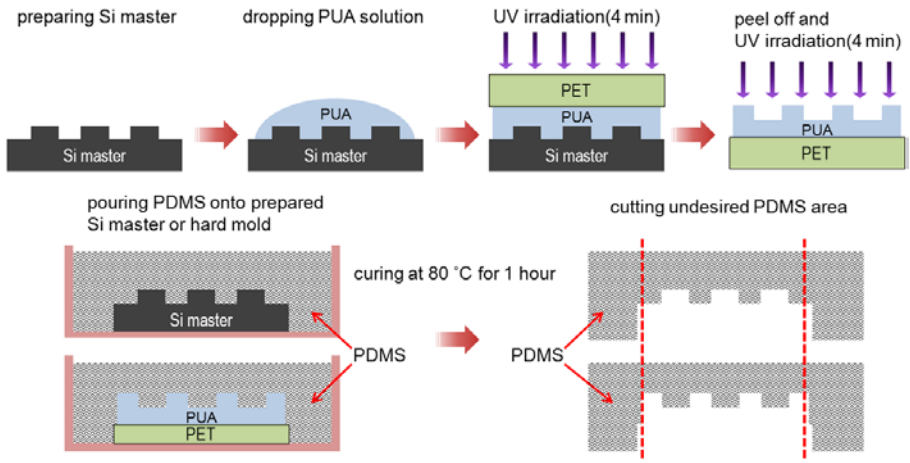

Figure 2.3 A schematic diagram of preparation of hard and soft molds

2.3.3 Hydrophobic surface treatment with a self-assembled monolayer

A hydrophobic silicon dioxide surface was prepared by the following procedure. To facilitate rich hydroxyl groups on a Si / SiO_2 surface, the silicon dioxide substrate was cleaned with UV-ozone treatment for 10 min, rinsed with DI water and annealed at 120 ˚C for 10 min. The surface of SiO_2 substrate was hydrophobically modified by immersing the Si / SiO_2 substrate in 2mM octadecyltrichlorosilnae (OTS) solution (in hexadecane or toluene)

for 12 hours and repeatedly cleaned with organic solvents (i.e., chloroform, IPA and methanol) to remove residual OTS. After cleaning, the OTS-treated SiO_2 substrate was annealed at 120 ˚C for 10 min. Finally, OTS self-assemled monolayer (SAM) was deposited on Si / SiO_2 substrate. The hydrophobicity difference was shown by measuring contact angle of DI water drops on bare SiO_2 surface (39˚) and OTS-treated SiO_2 surface (109˚) (see Figure 2.4(a) and (b)).

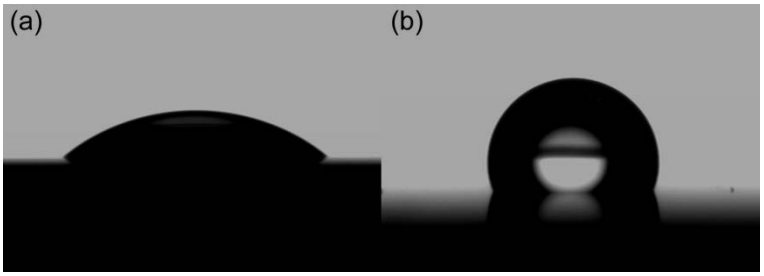

Figure 2.4 DI water drops on (a) bare Si / SiO_2 substrate and (b) OTS-SAM treated Si / SiO_2 substrate.

2.3.4 Current-voltage-luminance measurement

The current-voltage (*I-V*) characteristics were measured with a Keithley 236 source measurement unit, while the electroluminescence was measured with a calibrated Si photodiode (Hamamatsu, S5227-1010BQ) with a size of 10 mm × 10 mm placed at an angle normal to the device surface, assuming that the device was a Lambertian source. To detect a turn-on voltage of light-emitting

diodes, we use an ARC PD438 photomultiplier tube (PMT) with the Keithley 236 source measurement unit. The electroluminescence (EL) spectra and the Commission Internationale de L'Eclairage (CIE) color coordinates were measured with a Konica-Minolta CS-1000A spectroradiometer. The luminance and efficiency were calculated from the photocurrent signal of photodiode with a Keithley 2000 multimeter, and corrected precisely with the luminance from CS-1000A.

The chromatic characteristics were calculated from EL spectra measured by the CS-1000A spectrometer using the CIE 1931 color expression system. The tristimulus values *XYZ* can be calculated by following equations,

$$X = K_m \int_0^\infty \bar{x}(\lambda) P(\lambda) d\lambda \tag{2.1}$$

$$Y = K_m \int_0^\infty \bar{y}(\lambda) P(\lambda) d\lambda \tag{2.2}$$

$$Z = K_m \int_0^\infty \bar{z}(\lambda) P(\lambda) d\lambda \tag{2.3}$$

where, $P(\lambda)$ is a given spectral power distribution of emissive source, $\bar{x}$, $\bar{y}$ and $\bar{z}$ are the CIE standard color matching functions (see Figure 2.5) and K_m is the weighing constant (683 lm W^{-1}). From the tristimulus values, the CIE color coordinates calculated by following equations,

$$x = \frac{X}{X+Y+Z} \tag{2.4}$$

$$y = \frac{Y}{X+Y+Z} \tag{2.5}$$

$$z = \frac{Z}{X+Y+Z} \tag{2.6}$$

Any color can be plotted on the CIE chromaticity diagram.

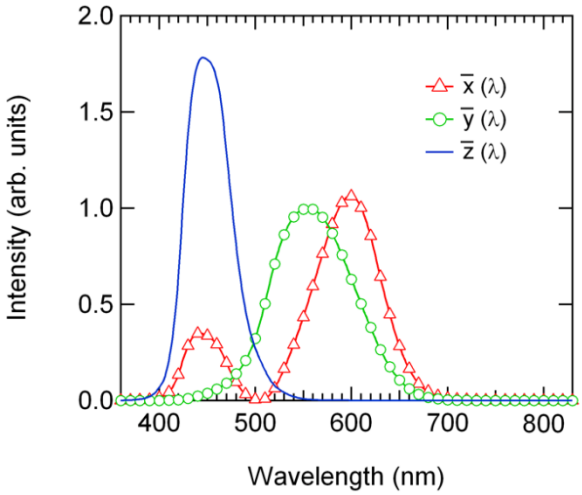

Figure 2.5 The CIE standard observer color matching functions

2.3.5 Emission efficiency calculation

To evaluate the emission properties of light-emitting diodes, the commonly employed efficiencies are the external quantum efficiency (EQE), the luminous efficiency (LE) and the power efficiency (PE).

The external quantum efficiency can be defined by the following equation.

$$\mathrm{EQE} = \frac{number\ of\ emitted\ photons}{number\ of\ injected\ electrons}(\%)$$

Typically, QLEDs or OLEDs emit light into the half plane due to the metal contact. Without any modification for increasing out-coupling efficiency,

over 80% of the emission can be lost to internal absorption and wave-guiding in a simple planar light-emitting device.

Since human eye has different spectral sensitivity in visible area, the response of the eye is standardized by the CIE in 1924 (see $\bar{y}$ in Figure 2.5). The luminous efficiency weighs all emitted photons according to the photopic response of human eye. The difference is that EQE weighs all emitted photons equally. LE can be expressed by the following equation.

$$\text{LE} = \frac{luminance}{current\ density}(cd\ A^{-1})$$

The luminance value (cd m^{-2}) can be easily measured by the commercial luminance meter (CS-1000A in this thesis).

The power efficiency is the ratio of the lumen output to the input electrical power as follows,

$$\text{PE} = \frac{luminous\ flux}{electrical\ power}(lm\ W^{-1})$$

The EQEs can be useful to understand the fundamental physics for light emission mechanism, while the PEs can be useful to interpret the power dissipated in a light-emitting device when used in a display application [53].

2.3.6 Angular dependent electroluminescence measurement

Angular dependent EL intensity and spectra were measured from 0° to 90° in 10° increments using an optical fiber and an Acton Spectro-275 monochromator combined with an ARC PD438 PMT on a rotation stage. A schematic diagram of this measurement system is depicted in Figure 2.6.

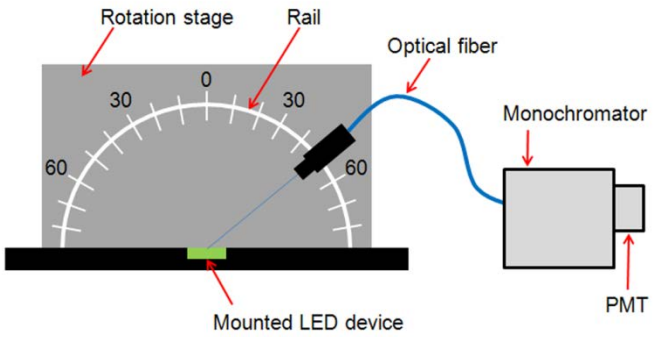

Figure 2.6 A Schematic diagrams for the angular dependent electroluminescence measurement

2.3.7 Electroluminescence measurement under bending condition

A QLED was placed on bending machine which controls and displays the bending distance of the QLED. EL spectra and luminance were measured with a Konica-Minolta CS-1000A spectroradiometer in the normal direction of the light emitting plane. The schematic diagram of bending measuring system is displayed in Figure 2.7(a).

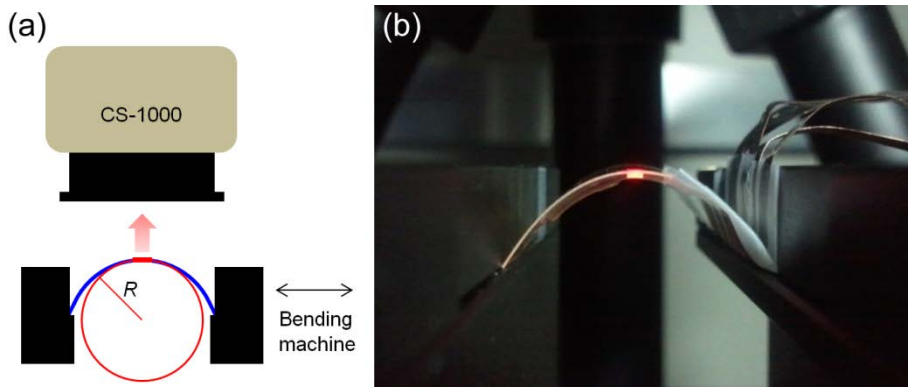

Figure 2.7 (a) A schematic diagram of bending radius dependent electroluminescence measurement (b) A photograph of a turned-on QLED device mounted on bending machine

2.3.8 Contact angle measurement and work of adhesion calculation

We measured the contact angles and calculated the work of adhesion values with the following harmonic-mean equation [54],

$$W_{1,2} = 4\left(\frac{\gamma_1^d \gamma_2^d}{\gamma_1^d + \gamma_2^d} + \frac{\gamma_1^p \gamma_2^p}{\gamma_1^p + \gamma_2^p}\right) \tag{2.7}$$

where $W_{1,2}$ is the work of adhesion between materials 1 and 2, γ is surface energy, and the superscripts of d and p are for the dispersion and polar components. Combining the Young's equation relating the equilibrium contact angle to the tensions at three-phase contact point [55] and the equation derived

by Owens and Wendt for the interfacial energy between liquid and solid [56] yields the following equation [57],

$$\gamma_l(1+\cos\theta) = 2(\gamma_s^d\gamma_l^d)^{0.5} + 2(\gamma_s^p\gamma_l^p)^{0.5} \quad (2.8)$$

where θ is the equilibrium contact angle and the subscripts of s and l are for the solid and liquid surfaces, respectively. The contact angles were measured by using low-bond axisymmetric drop shape analysis (LBADSA) method [58] which is based on the fitting of the Young-Laplace equation to the droplet images with polar and non-polar probing liquids (DI water and ethylene glycol, respectively).

2.3.9 Other Characterization Methods

UV-Vis. Spectroscopy: The transmission and absorption spectra were measured with DU-70 UV/Vis Scanning Spectrophotometer (Beckman Coulter, Inc.) or Agilent 8454 UV-Vis. diode array spectrometer. In case of solution, materials were dissolved in toluene or chlorobenzene. For the film measurement, materials were spin-coated or evaporated thermally in the thickness of ~50 nm on quartz substrate. The reflectance spectra were measured by a Varian Cary 5000 spectrophotometer. The average transmittance (T_{avg}) was calculated by the following equation.

$$T_{avg} = \frac{\int_{\lambda_1}^{\lambda_2} T(\lambda)\mathrm{d}\lambda}{\lambda_2 - \lambda_1} \quad (2.9)$$

where $T(\lambda)$ is the transmittance as a function of the wavelength, T_{avg} was usually calculated by integrating $T(\lambda)$ from 400 nm (λ_1) to 800 nm (λ_2).

Atomic Force Microscopy (AFM): Topography of each film was measured by XE-100 (Park Systems) AFM System. Most of the films were measured in non-contact mode with NCHR probe tip (320 kHz, 42 N m^{-1}) followed by image processing in XEI v.1.7.1.

Transmission electron microscopy (TEM): The TEM images of the QDs were obtained using a JEOL JSM-890 at 200 KV to analyze their average size and size distribution. The energy dispersive x-ray (EDX) spectra of QDs were acquired through Si-Li detector of Oxford INCA Energy attached on main body of TEM. Low-coverage samples were prepared by placing a drop of a dilute hexane dispersion of QDs on a copper grid (300 mesh) coated with an amorphous carbon film.

Fluorescent optical microscopy (FOM): The FOM images were obtained using a confocal imaging system consisting of a Nikon Eclipse E600-POL microscope, a Nikon DXM1200F camera, a Y-EL EPI-Fluorescence attachment and a mercury lamp. Filter blocks were composed of excitation filter, dichromic mirror and barrier filter. For red, green and blue image, excitation filters pass 540–580, 465–495 and 330–380 nm regions, and dichromic mirrors reflect over 595, 505 and 400 nm and barrier filters pass 600–660, 515–555 and 420 nm regions, respectively.

Energy Level Measurement: The highest occupied molecular orbital (HOMO) energy levels of organic materials were measured by Model AC-2

Photoelectron Spectrometer (RKI Instruments) in ambient atmosphere at room temperature.

Sheet resistance measurement: The sheet resistances of conductive films were measured by FPP-5000 4-point probe (Changmin Tech Co., Ltd.) at a 0.1 mA current flow.

Chapter 3. Soft-Contact Transplanted Quantum Dots for Light-Emitting Diodes

3.1 QD-Layer Deposition by Soft-Contact Transplanting

3.1.1 QD transplanting methods

To make QD layer patterned, various printing methods such as ink-jet printing, contact printing, and transfer printing have been reported [29,59]. Among these printing techniques, contact printing or transfer printing by using PDMS as a stamp has advantages on making conformal contact with substrate surfaces with its low adhesion properties. In addition, the QLEDs fabricated via these methods exhibited moderate device performances with fine patterns, compared to other printing techniques [16]. Despite these advantages, PDMS, the elastomeric stamp swells up and contorted by most organic solvents used for dispersing QDs (see Figure 3.1(a–d)). When green QD solution were spin-deposited to bare PDMS surface, very non-uniform surface as shown in Figure 3.1(a) was observed and from the coated QD layers, the transferred QD layers on glass / ITO substrate was also non-uniform morphology. Hardened PDMS surface by 10-min UV-ozone treatment showed better resistance, however, the morphology of spin-coated QDs on UV-ozone treated PDMS was not good enough to deposit uniform QD layers (see Figure 3.1(c,d)).

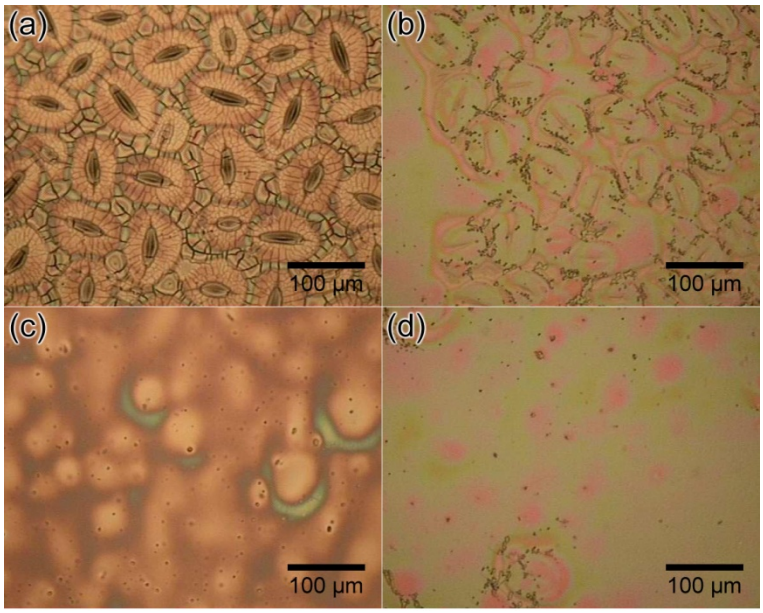

Figure 3.1 Optical microscope images of (a,b) spin-coated QDs on (a) bare PDMS and (b) UV-ozone treated PDMS and (c,d) transferred QD layers on glass/ITO using (c) bare and (d) UV-ozone treated PDMS.

To overcome the swelling problem, several methods have been tried such as coating parylene-C or SU-8 photoresist on PDMS as a protection layer [8,16,17], and indirect deposition of QDs on the PDMS stamp [14]. However, additional processes for preventing PDMS from swelling make the technique more complicated. Drop-casting method has advantage of depositing QD film on a desired substrate, but it needs over-saturated solvent vapor condition and additional time for solvent dewetting as to get self-assemble QD nanoparticles as compact structure [14]. Compared to this, spin-casting is fast and processible in ambient air condition.

For the transplanting process, the QD dispersion in hexane (10 mg ml^{-1}) was spin-coated on an OTS-treated SiO_2 substrate (donor substrate) at a rate of 4,000 rpm for 30 s. For better adhesion between the two surfaces of QDs and PDMS, the PDMS stamp was UV-ozone treated for 4 min and attached on the donor substrate of Si / SiO_2 / OTS / QDs. PDMS molds were pre-patterned by the above described method (Chap. 2.3.2). PDMS contacted in a conformal way without a pressure. By peeling off PDMS from the donor substrate, the QD layers was transferred on the devices substrate of glass / ITO / PEDOT:PSS / poly-TPD. The used chemical structures and schematics of this procedure were shown in Figure 3.2 and Figure 3.3, respectively. Transplanting process was conducted under ambient conditions without an additional heat and pressure.

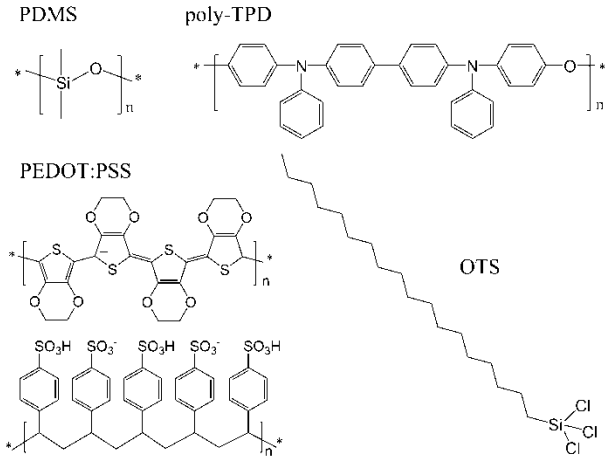

Figure 3.2 The chemical structures used in QD transplanting method

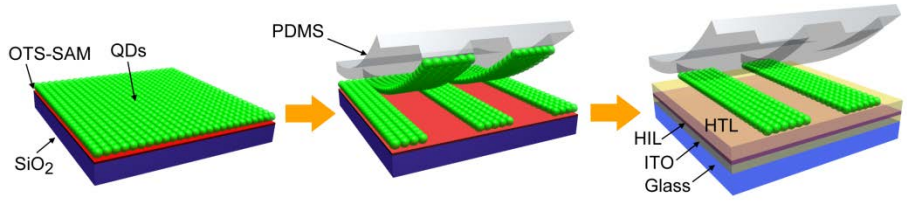

Figure 3.3 Schematics on the soft-contact transplanting of colloidal quantum dots on versatile soft organic layers. No additional heat and pressure were applied during the entire transfer process.

3.1.2 Film property of transplanted QD layers

The transplanted QD patterns on glass / ITO / PEDOT:PSS / poly-TPD substrates were characterized with FOM and TEM. Figure 3.4(a–c) shows the FOM images of red, green, and blue QD line patterns with different line width of 6, 4, and 2 μm. From the FOM images, any noticeable defect in the transplanted line or dot patterns is not observed. To better understand the morphology of transplanted QD pattern lines, we have characterized the QD layers with TEM (Figure 3.4(d–f)). To prepare a TEM sample, the glass / ITO / PEDOT:PSS / poly-TPD / QDs substrates were carefully immersed in petri dish filled with DI water. Because the PEDOT:PSS layer was dissolved with DI water, the film of poly-TPD / QDs was floated on DI water surface and caught by TEM grid. QD layers prepared by both spin-casting and transplanting method show homogeneous and uniform QD morphology, but small vacancies with a size of 20–50 nm in diameter are observed in the case of transplanted QD layers (see Figure 3.4(d) and (e)). The edge roughness of

transplanted QD layer is estimated at most 80 nm (see Figure 3.4(f)). The defects (i.e., QD vacancies or non-uniform edge line) within QD layers seem to originate from the weak particle-particle interaction forces among assembled QD layers, but we believe they can be overcome through optimizing the transplanting conditions, such as transplanting temperature, pressure, and detaching or removing speed.

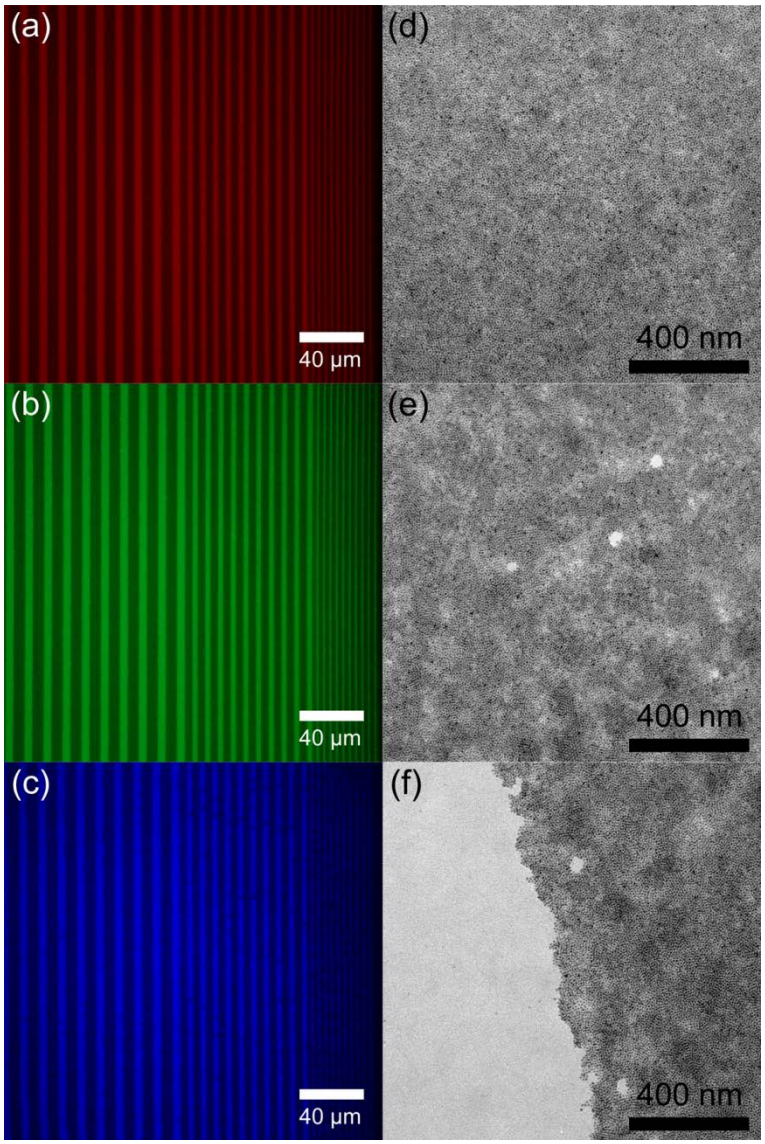

Figure 3.4 Fluorescent optical microscope (FOM) images of patterned (a) red, (b) green and (c) blue QD line patterns transplanted on poly-TPD / PEDOT:PSS / ITO / glass substrates. TEM images of QD layers deposited on poly-TPD / PEDOT:PSS / ITO / glass substrates by (d) conventional spin-coating method and (e) transplanting method, and (f) the edge region of transplanted QD layer.

QD transplanting on already transplanted QD layers was also tried with green QDs. First, QD layers were transplanted on the glass / ITO / PEDOT:PSS / poly-TPD substrate with a certain direction and then again, QD layers were transplanted on the resulting substrate with the 90˚ tilt direction. Figure 3.5 showed FOM and AFM images of double transplanted QD layers.

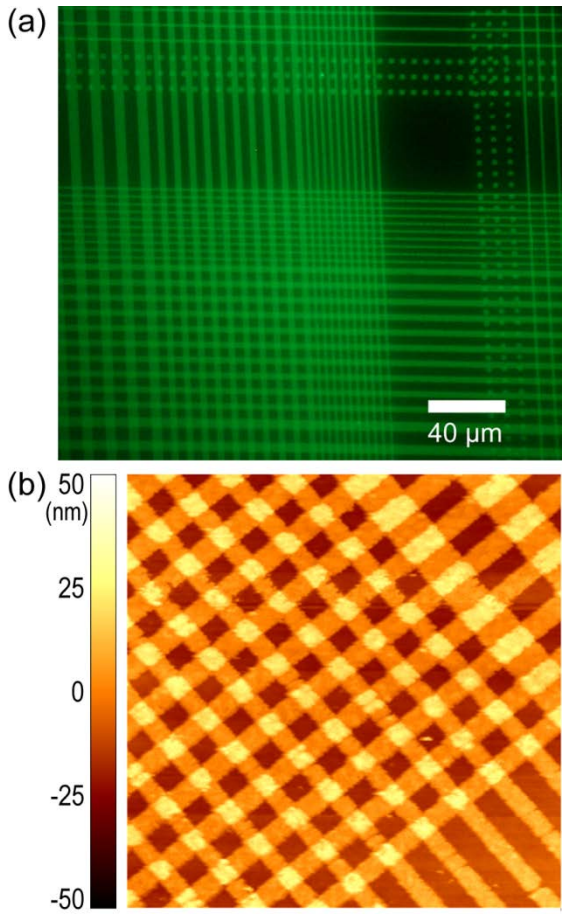

Figure 3.5 The (a) FOM and (b) AFM images of double transplanted QD layers

3.1.3 Characteristics of red, green, and blue QLEDs using QD transplanting

To evaluate transplanted QLED performances, we fabricated red, green and blue QLEDs using spin coating and transplanting methods. Figure 3.6 plots current density-voltage and luminance-voltage characteristics of red, green and blue QLEDs with transplanted or spin-coated QD active layers. QLEDs with transplanted QD active layers show lower turn-on voltage (red, green and blue: 4.7 V) and higher current density under the same applied voltage when compared with spin-deposited QLEDs, which seems to originate from the current leakages through the vacancies within the transplanted QD active layers. However in the case of green QLEDs, both types of devices show similar device characteristics in terms of current density, turn-on voltage, and luminance, indicating that the transplanted QD active layers can have the same morphology as the conventional spin-coating method and the charge carrier leakage pathways (i.e., vacancies) can be minimized by the optimization of the transplanting method.

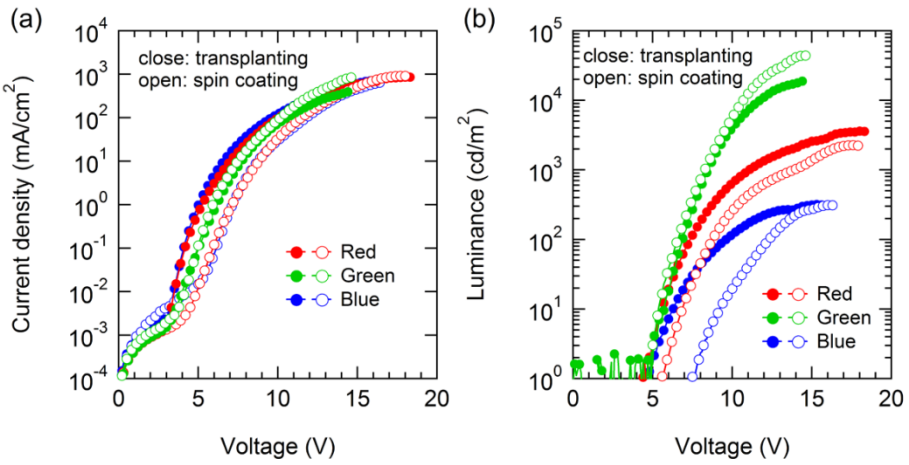

Figure 3.6 (a) Current density-voltage and (b) luminance-voltage characteristics of red, green and blue QLEDs with (close) transplanted QD active layers and with (open) spin-deposited QD active layers.

Figure 3.7(a) compares the electroluminescence (EL) spectra of QLEDs with transplanted and spin-coated active layers. Both types of devices exhibit color-saturated narrow EL emission (Gaussian FWHM ~30 nm) with a peak emission wavelength at 448, 525, and 639 nm for blue, green and red QLEDs, respectively, representing that QDs are the major exciton recombination center within devices. Particularly, in the case of green QLEDs with transplanted QD active layer, any noticeable parasitic emission from neighboring charge transport layers (i.e., poly-TPD or TPBi) is not observed.

Figure 3.7(b) shows external quantum efficiency (EQE) of QLEDs with transplanted and spin-coated QD active layers. Although the peak EQEs of transplanted QLEDs (red: 0.88, green: 1.8 and blue: 0.18%) were slightly lower than the peak efficiencies of QLEDs with spin-casted QD active layers

(red: 1.9, green: 2.1 and blue: 0.095%), both types of QLEDs shows comparable EQEs in the practicable current density regime (i.e., 10–100 mA cm^{-2}).

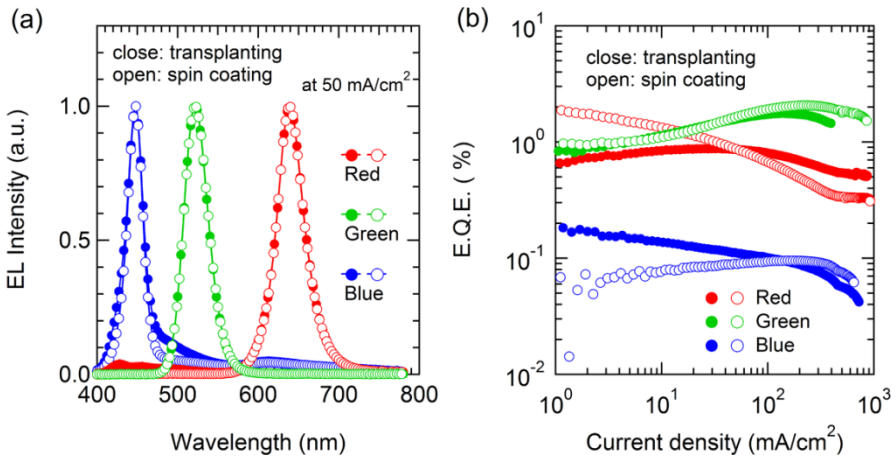

Figure 3.7 (a) Electroluminescence (EL) spectra and (b) external quantum efficiency (EQE) of red, green and blue QLEDs with (close) transplanted QD active layers and with (open) spin-deposited QD active layers.

However, in the case of B and R-QLEDs with transplanted QD active layers, the broad parasitic emissions were slightly observed. When those devices were operated at lower current density, the portion of parasitic emission was larger. CIE coordinates of transplanted devices at a current density of 0.5 mA cm^{-2} changed much from those of the devices at a current density of 5 mA cm^{-2}, however, color shifts in spin-coated devices were negligible (see Figure 3.8(a)). In Figure 3.8(b), the EL spectra of red devices at low current density and poly-TPD EL emission of the OLED device

without QD layers (structure: glass / ITO / PEDOT:PSS / poly-TPD / TPBi / LiF / Al) are compared. Poly-TPD EL emission was found to correspond to parasitic emission residing at 400–550 nm. Those parasitic emissions were originated from the unexpected exciton formation within poly-TPD layers as a result of the electron leakages from TPBi to poly-TPD through the vacancies.

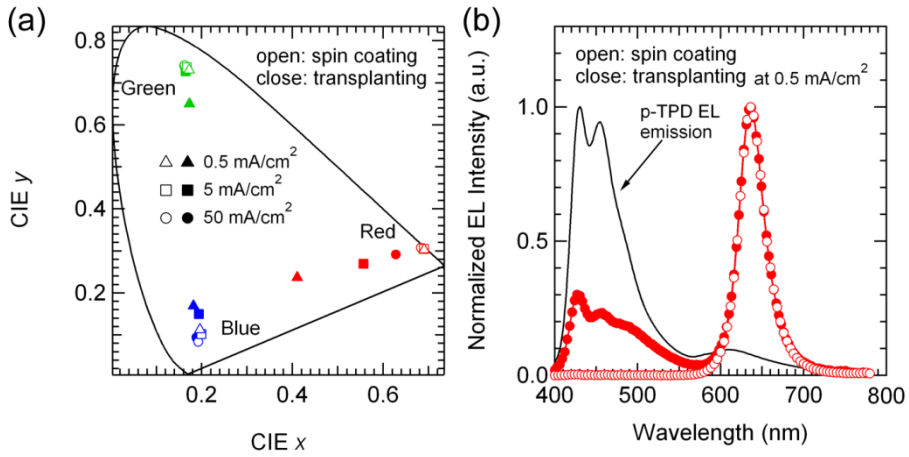

Figure 3.8 (a) CIE color coordinates of red, green and blue QLEDs with (open) spin-coated and (close) transplanted QDs at various current density values. (b) EL spectra of red devices using spin-coating and transplanting methods at a current density of 0.5 mA cm^{-2} and poly-TPD EL spectrum.

3.2 QD Transplanting on Vacuum-Deposited Hole Transporting Materials

We have few choice of polymer or cross-linkable hole transporting materials possessing low values of the highest occupied molecular orbital (HOMO) energy level required for facilitated hole injection into QDs. Since the valence band (VB) of QD (< -6.5 eV) is much lower than general hole transporting organic molecules or polymers (> -6 eV), the lower HOMO energy level of hole transporting layer (HTL) serves more efficient hole injection into QDs. Another reason for using baked HTL in that paper was that high pressure (196 kPa) was applied to the HTL during transferring QDs. Although we have a plenty of choices of small molecule HTLs possessing low HOMO values, it is impossible for vacuum-deposited HTLs to endure such high pressure during the transfer process. In order to transfer and pattern QDs on a soft organic layer, therefore, a printing process without high pressure is required. To confirm whether pressure affects favorably or not, we compared the morphologies of the QD-transplanted layers on the vacuum deposited HTL (TCTA) using QD-transplanting method without pressure and with a pressure of 196 kPa (see Figure 3.9(a) and (b)). In Figure 3.9(b), a lot of cracks of QD layers were observed. We show QD transplanting technique which is a method of transferring a patterned QD layer onto a vacuum-deposited small molecule HTL without pressure, and demonstrate bright and efficient red, green and blue QLEDs via this method.

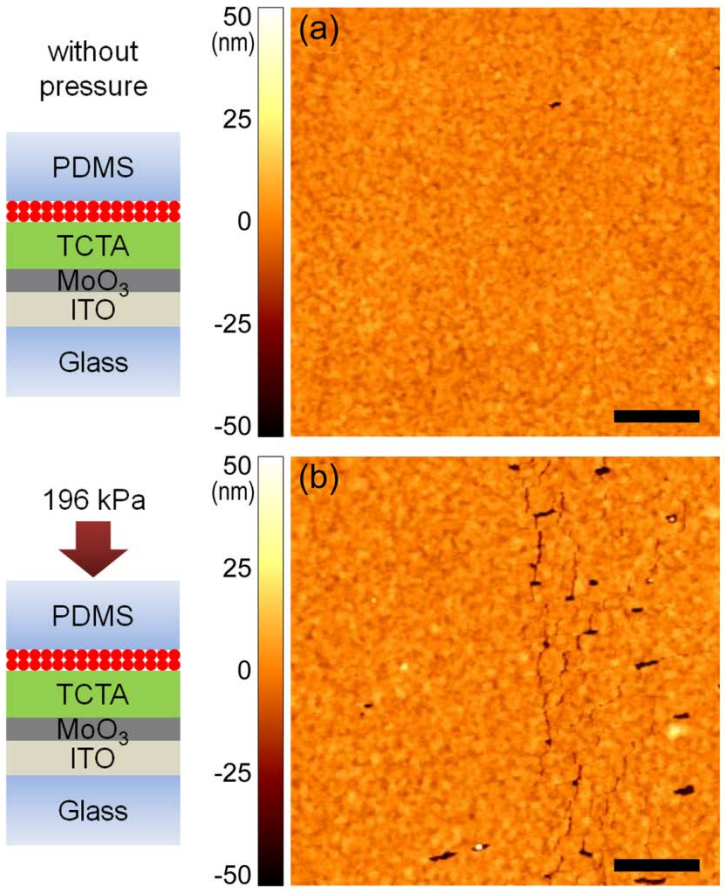

Figure 3.9 The AFM images of the QD-transplanted layers on the vacuum-deposited HTL (TCTA) using QD-transplanting method (a) without pressure and (b) with a pressure of 196 kPa.

3.2.1 Patternability difference on vacuum-deposited HTMs

As mentioned priorly, a HTL possessing low HOMO energy level is required for efficient hole injection into QDs. For this, we chose three different widely-used organic HTMs possessing low HOMO levels based on carbazole, which were N,N'-dicarbazolyl-3,5-benzene (mCP), 4,4'-N,N'-dicarbazole-biphenyl (CBP) and 4,4',4''-Tri(N-carbazolyl)triphenylamine (TCTA) and their HOMO energy values were 5.93, 5.97, and 5.70, respectively, measured with an AC-2 photoelectron spectrometer. We transplanted green QDs onto each hole transport organic layer by using the PDMS stamp which has line-and-space patterns with the widths of 6, 4, and 2 μm, and observed with a FOM to examine the wettability and patternability of QDs. As shown in the FOM images in Figure 3.10(a–c), the transplanted QDs on each HTL shows clear differences in terms of patternability; In case of using mCP, QD stripes were non-uniformly and sparsely patterned, thus, they shows weak fluorescence (Figure 3.10(a)). For the case using CBP, the patterns were more uniform than those at the mCP sample, but the edges of the patterns were quite rough and broken partly in the narrow stripes (Figure 3.10(b)). On the other hand, when we used TCTA as the HTL, QD stripes by transplanting method were highly uniform and had fine edges for all widths of patterns without any noticeable defect (Figure 3.10(c)). Insets in each figure shows the magnified FOM images of 4-μm-width stripes, which closely shows the difference of transplanting morphology according to the underlying organic layer as mentioned above. After transplanting QDs on each HTL, the PDMS stamps

were also observed with a FOM to ascertain the existence of residual (i.e, untransferred) QDs. As can be expected, a lot of QDs remained on the PDMS stamped onto mCP, while little QDs existed on the stamp used onto TCTA (see Figure 3.10(d–f)).

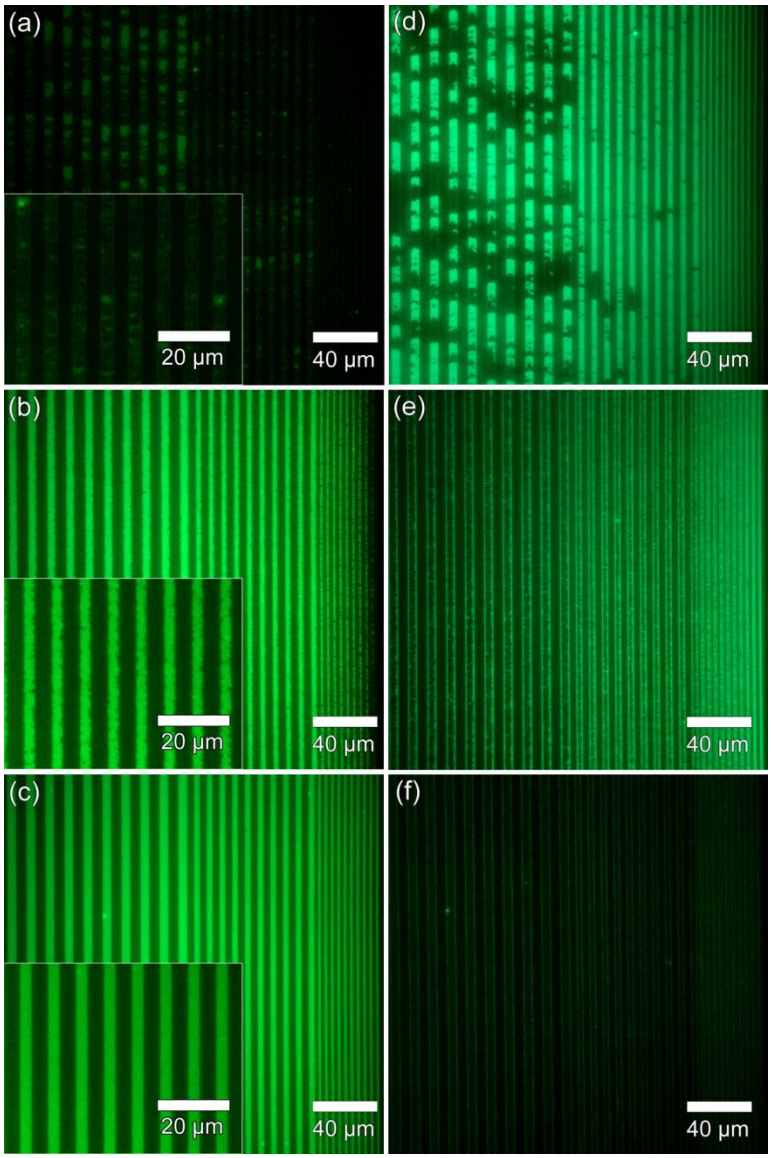

Figure 3.10 The fluorescent optical microscopy (FOM) images of stripe-patterned green QDs on various organic hole transport materials (HTMs) ((a) mCP, (b) CBP and (c) TCTA) using the soft-contact transplanting method. The FOM images of residual QDs on the PDMS stamps after transplanting green QDs onto (d) mCP, (e) CBP and (f) TCTA.

In order to find out the reason of these drastic differences depending on the organic layer, we measured the contact angles (Figure 3.11(a–h)) and calculated the work of adhesion values. Measured contact angles with dispersive and polar solvents, and calculated surface energies were summarized in Table 3.1.

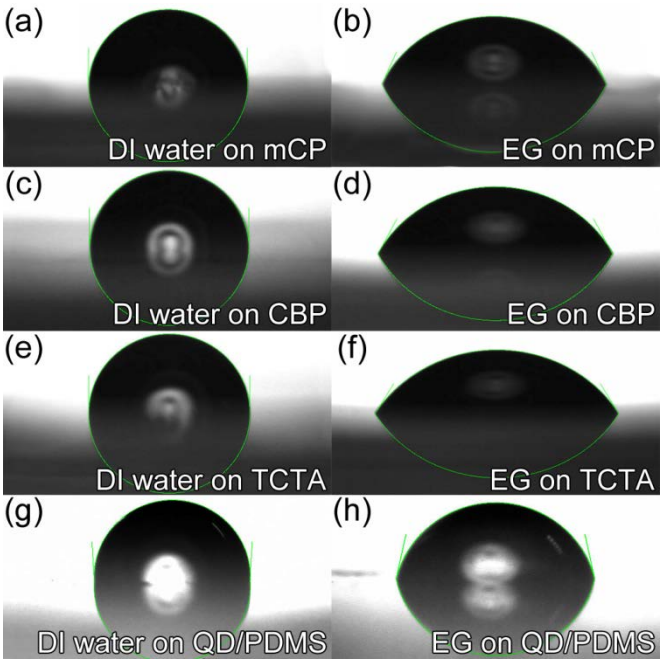

Figure 3.11 The liquid drop images of (a,c,e,g) polar (DI water) and (b,d,f,h) non-polar solvents (ethylene glycol) on the various hole transport materials of (a,b) mCP, (c,d) CBP and (e,f) TCTA, and on the (g,h) QD/PDMS to measure the contact angles for the surface energy calculation.

Table 3.1 Contact angles and surface energies of used hole transport layers and QD (stabilized with oleic acid) layer on PDMS, and calculated work of adhesion between HTLs and QDs on PDMS stamp.

HTL	Contact angle (°)		γ^d (mJ m^{-2})	γ^p (mJ m^{-2})
	DI water	Ethylene glycol		
mCP	87.9	65.0	4.91	1.32
CBP	89.1	61.7	6.60	0.72
TCTA	90.7	58.9	8.47	0.28
QDs on PDMS	97.0	77.3	3.82	0.84

Note: γ^d, non-polar part of surface energy; γ^p, polar part of surface energy. Work of adhesion between each HTL and QDs.

The calculated work of adhesion values between each HTL and the QDs on PDMS, or $W_{mCP,QD}$, $W_{CBP,QD}$, and $W_{TCTA,QD}$, were 10.7, 11.2, and 11.4 mJ m^{-2}, respectively, as compared in Figure 3.12. From this result, mCP film has weak adhesion with QDs compared to other films and therefore a poor QD film on mCP was produced by transplanting method. Similarly $W_{TCTA,QD}$ is slightly higher than $W_{CBP,QD}$ resulted in much better film formation as shown in the FOM images.

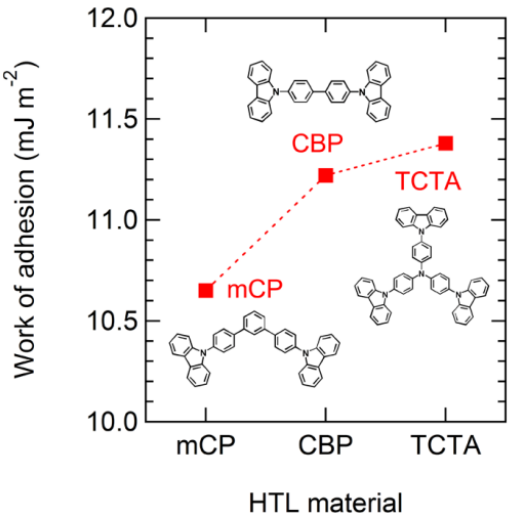

Figure 3.12 Plots of calculated work of adhesion values between HTMs and QDs. (inset: chemical structures of HTMs).

3.2.2 Electroluminescence Characteristics of green QLEDs using transplanted QD layers on various HTLs

Although patterned QDs on mCP or CBP showed rough shapes, we also fabricated and characterized the green QLED devices with those HTLs (see Figure 3.13(a–d)). Because the coverages of transplanted QDs were good in the order of TCTA, CBP and mCP, the current density at the same voltage showed low in the same order. (see Figure 3.13(a)). Due to the low emission efficiency occured at the interface of organic HTL and ETL, the devices which have good coverage of tranplanted QDs showed high luminous efficiency (LE) (see Figure 3.13(c)). Since QDs were hardly transplanted on

mCP, we could not observe any emission from green QDs but blue emission originating from the adjacent the organic layers (Figure 3.13(d)). In case of CBP on which QDs were partly transplanted, the device emitted green color mainly from QDs and a little blue emission from adjacent organic layers, which are attributed to incomplete QD-deposition on the CBP layer. The device using TCTA showed good performances compared to other HTMs.

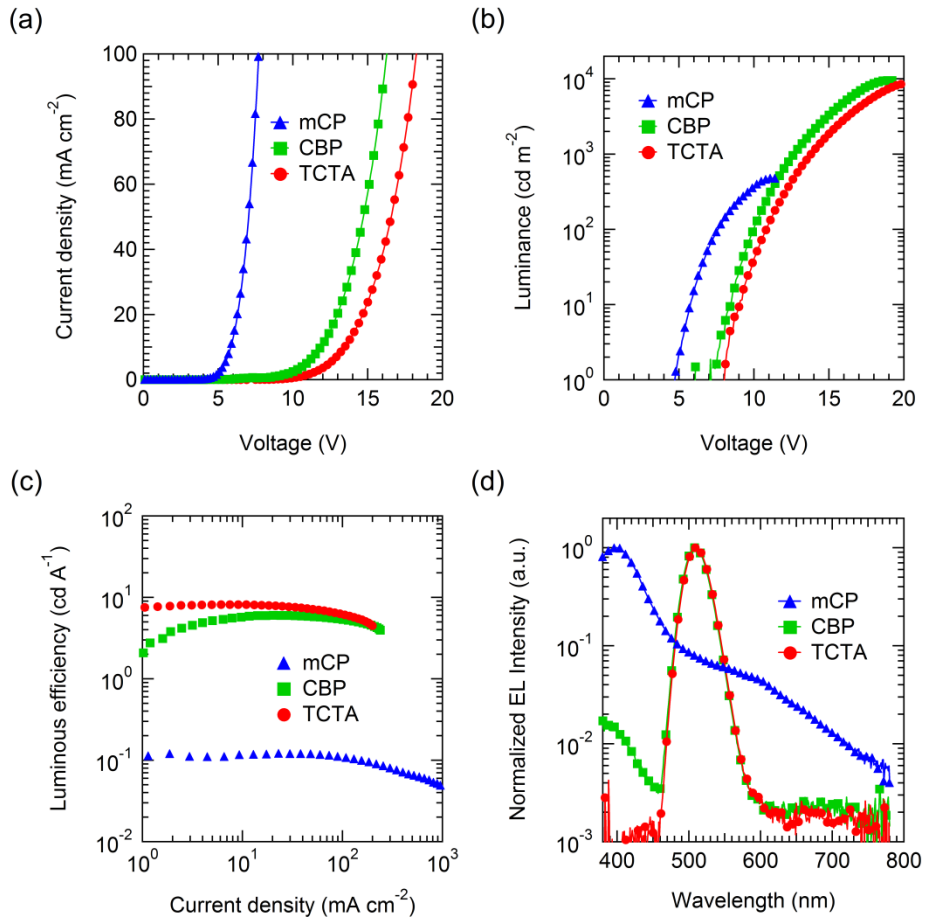

Figure 3.13 The device performances of green QLEDs with mCP, CBP, and TCTA as the HTL by using the transplanting method, in terms of (a) current density-voltage and (b) luminance-voltage characteristics, (c) external quantum efficiency-current density curves, and (d) normalized electroluminescence spectra in log-scale measured at 5 mA cm^{-2}.

3.2.3 Electroluminescence Characteristics of red, green and blue QLEDs using transplanted QD layers on TCTA

Figure 3.11(a–d) shows the device performances of the QLEDs using transplanted QDs on TCTA. From the current-voltage and luminance-voltage characteristics shown in Figure 3.14(a) and (b), we obtained that the maximum luminance of 2,500, 14,100, and 265 cd m^{-2} for red, green and blue QLEDs, respectively. The maximum LE values of the transplanted red, green and blue QLEDs are 1.83, 8.07 and 0.19 cd A^{-1} as shown in Figure 3.14(c), which correspond to 1.93, 2.33 and 0.32% in the external quantum efficiency (EQE), respectively. These performances of the transplanted devices are comparably high with the paper reported the highest efficiency and brightness for all colors [22]. Compared to above results of QLEDs using transplanted QDs on poly-TPD HTL (red: 0.88%, green: 1.8% and blue: 0.18%), these results showed improved efficiency values. Also, the turn-on voltages were lowered than those devices using poly-TPD HTL. These better performances were attributed to more efficient hole injection due to lower HOMO level of TCTA than that of poly-TPD. As shown in Figure 3.14(d), all devices exhibit deeply saturated colors and narrow EL emission with Gaussian full-width-at-half-maximum (FWHM) about 30 nm, and their peak emission wavelengths are 637, 519 and 436 nm for red, green and blue QLEDs, respectively.

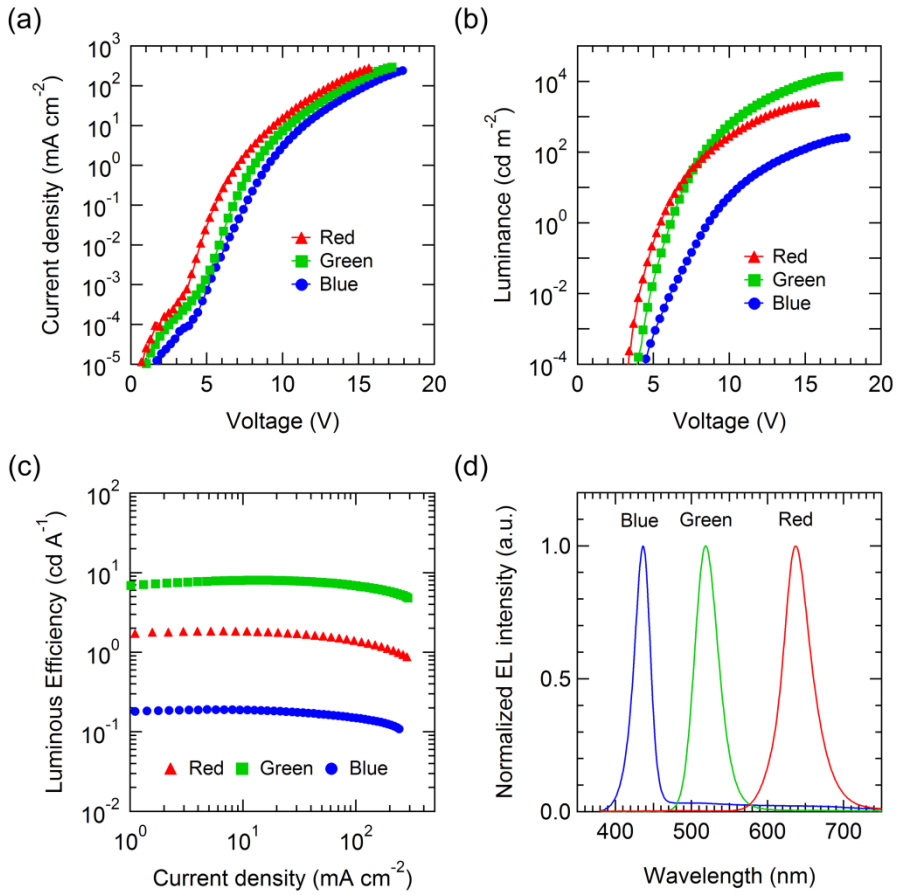

Figure 3.14 Optical and electrical characteristics of red, green, and blue QLEDs employing transplanted QD active layers. (a) current density-voltage, (b) luminance-voltage characteristics, (c) luminous efficiency-current density, and (d) normalized EL spectra of QLEDs at a current density of 50 mA cm^{-2}.

Moreover, most of the emission originated from QD layers owing to the good patterning property of TCTA, resulting in saturated colors, high color purity, and wide color gamut; The CIE coordinates of (0.68, 0.31), (0.15, 0.72) and (0.19, 0.06) for R, G and B devices mostly covers the color gamut of the

National Television Standards Committee (NTSC) 1953 color space (see Figure 3.15). The color gamut reached 105% of the NTSC color space. The device performances of transplanted red, green and blue QLEDs are summarized in Table 2.

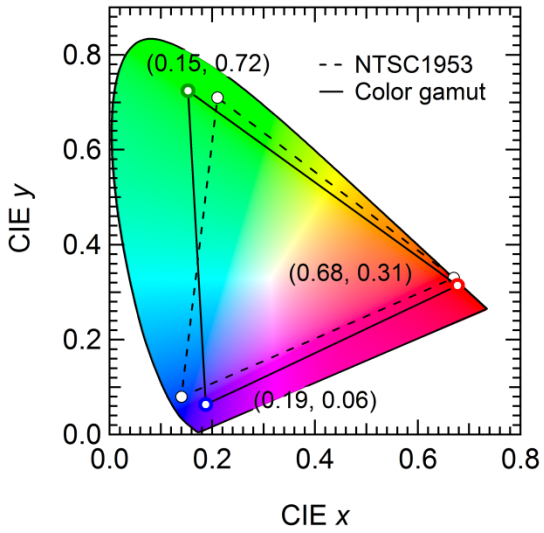

Figure 3.15 The CIE color coordinates of red, green, and blue QLEDs with TCTA using the transplanting method, and their color range compared with NTSC 1953 color gamut.

Table 3.2 The device performances of red, green and blue QLEDs with transplanted QD active layers between soft organic layers.

Color	Max. EQE (%)	Max. LE (cd A^{-1})	Max. luminance (cd m^{-2})	V_{on} (V)	EL λ_{max} (nm)	CIE color coordinates (x, y)
Red	1.93	1.83	2,500	3.4	436	(0.68 ,0.31)
Green	2.33	8.07	14,102	4.0	519	(0.15, 0.72)
Blue	0.32	0.19	265	4.5	637	(0.19, 0.06)

Note: Turn-on voltage (V_{on}) was detected by photomultiplier tubes.

3.3 QD Transplanting on the ZnO Electron Transporting Layer

3.3.1 Pressure-assisted QD-transplanting on ZnO layer

Recently, the inverted structure using ZnO electron transporting layer (ETL) showed good device performance compared to the standard structure. We also tried QD transplanting on ZnO layer. However, QDs were not transferred on ZnO with same transplanting condition (i.e. without pressure) as we conducted on the vacuum-deposited HTLs. Though soft organic material can be damaged by applying pressure on top of that, hard inorganic metal oxide is expected to endure that pressure. FOM images are shown in Figure 3.16(a-d). The clear differences were shown at the regions of 2 μm width pattern with various pressures. Cracks were found in the without-pressure and 1.2 MPa samples. However, any crack was not observed in the 0.1 and 0.25 MPa samples.

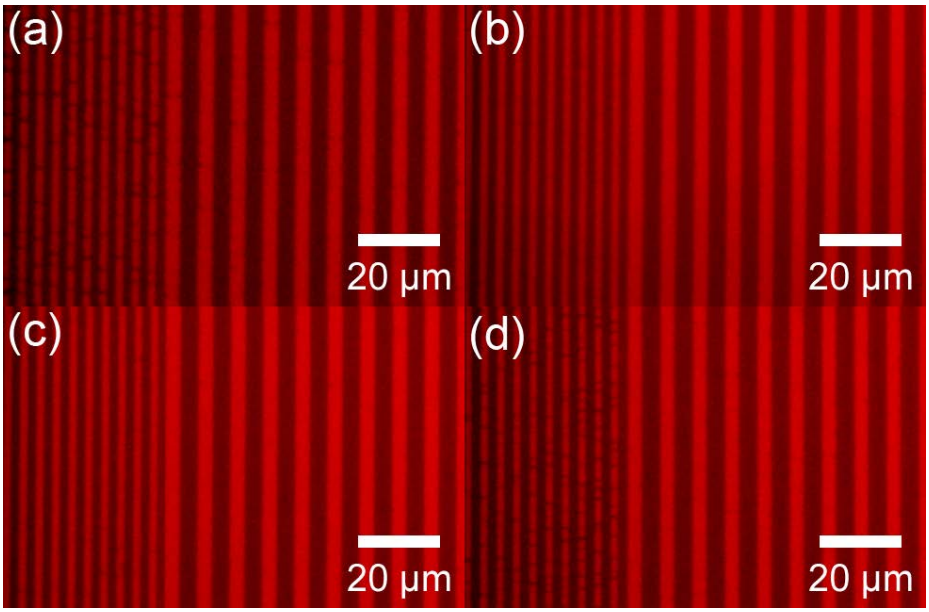

Figure 3.16 FOM images of stripe-patterned green QDs (a) without pressure and with various pressure of (b) 0.10 MPa, (c) 0.25 MPa and (d) 1.2 MPa.

For further investigation, the morphologies of 2 μm width patterns were measured by scanning electron microscope (SEM) as shown in Figure 3.17(a-d). The patternability differences were more clearly shown in the SEM images than in the FOM images.

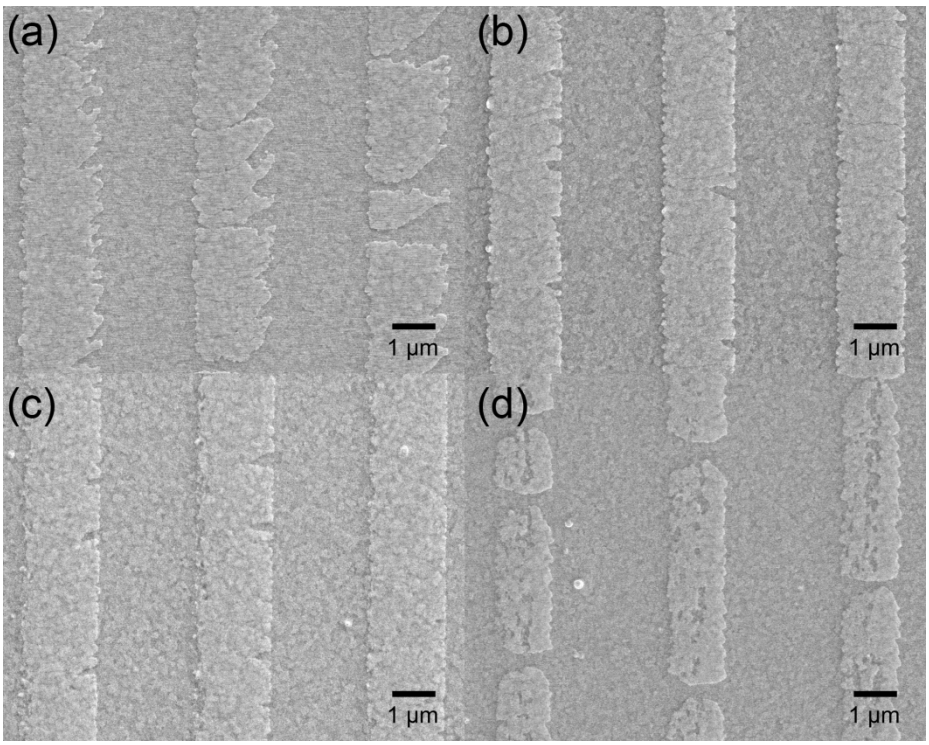

Figure 3.17 SEM images of stripe-patterned green QDs (a) without pressure and with various pressure of (b) 0.10 MPa, (c) 0.25 MPa and (d) 1.2 MPa.

3.3.2 Electroluminescence characteristics of red QLEDs using transplanted QD layer with various pressure conditions

Figure 3.18(a–d) shows the device performances of the QLEDs using transplanted QDs on ZnO. From the current-voltage and luminance-voltage characteristics shown in Figure 3.18(a) and (b), we obtained that the maximum luminance of 12,900, 26,200, and 860 cd m^{-2} for red, green and blue QLEDs, respectively. The maximum EQE values of the transplanted red, green and blue QLEDs are 6.3, 0.94 and 0.26% as shown in Figure 3.14(c), respectively.. As shown in Figure 3.14(d), all devices exhibit deeply saturated colors and narrow EL emission with Gaussian full-width-at-half-maximum (FWHM) about 30 nm, and their peak emission wavelengths are 636, 521 and 435 nm for red, green and blue QLEDs, respectively.

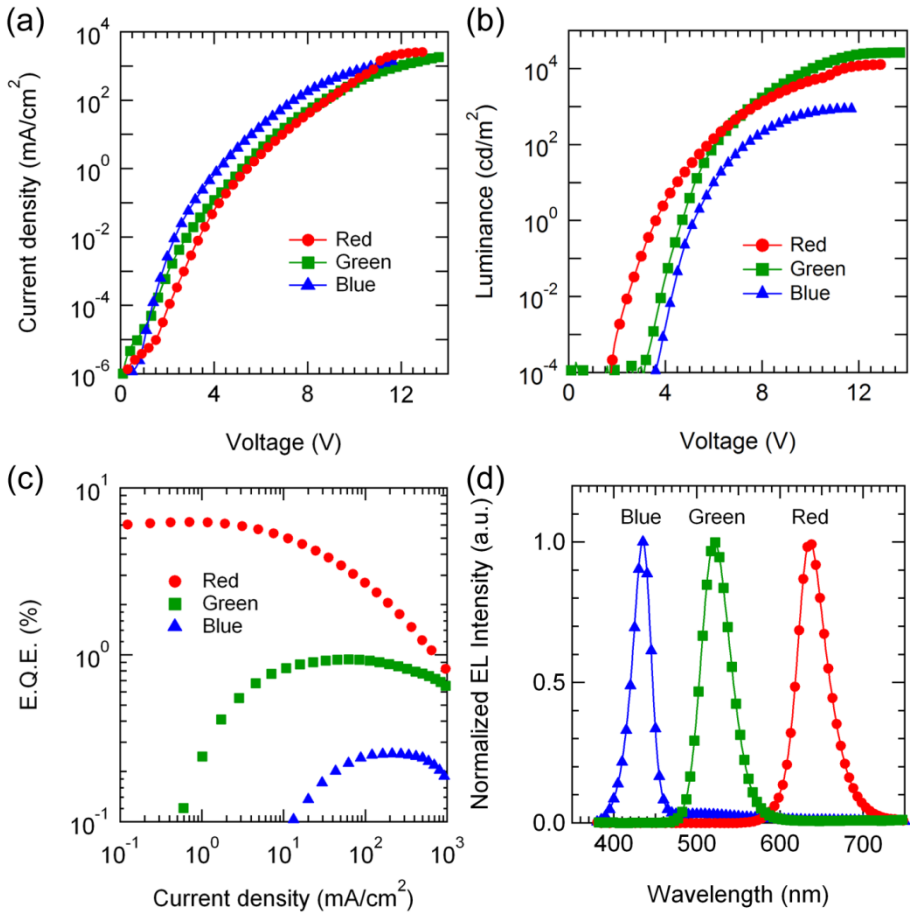

Figure 3.18 Optical and electrical characteristics of red, green, and blue QLEDs employing transplanted QD active layers on ZnO ETL. (a) current density-voltage, (b) luminance-voltage characteristics, (c) luminous efficiency-current density, and (d) normalized EL spectra of QLEDs at a current density of 50 mA cm^{-2}.

Chapter 4. Transparent and Flexible Quantum-Dot Light-Emitting Diodes

4.1 Transparent and Flexible QLEDs Using *p*-doped Graphene Electrode as an Anode

4.1.1 Preparation of graphene electrodes

Graphene electrodes for top contact were prepared by the following procedure. A 500 μm-thick PDMS substrate was UV-ozone treated for 10 min and attached to the PES / graphene substrate which was prepared by the above mentioned procedure (see Chapter 2.2). After contacting PDMS conformally on PES / graphene substrate, the PDMS substrate was peeled off quickly, then multilayer graphene films were detached from PES donor substrate. To verify graphene-transfer from PES to UV-ozone treated PDMS, we measured the contact angles (as shown in Figure 4.1(a–j)) and calculated the works of adhesion. The measured contact angles, the calculated surface energies and the works of adhesion were summarized in Table 4.1. Since the work of adhesion between graphene and UV-ozone treated PDMS (11.5 mJ m^{-2}) is larger than that between graphene and PES substrate (10.1 mJ m^{-2}), graphene sheets on the PES can be easily transferred to PDMS.

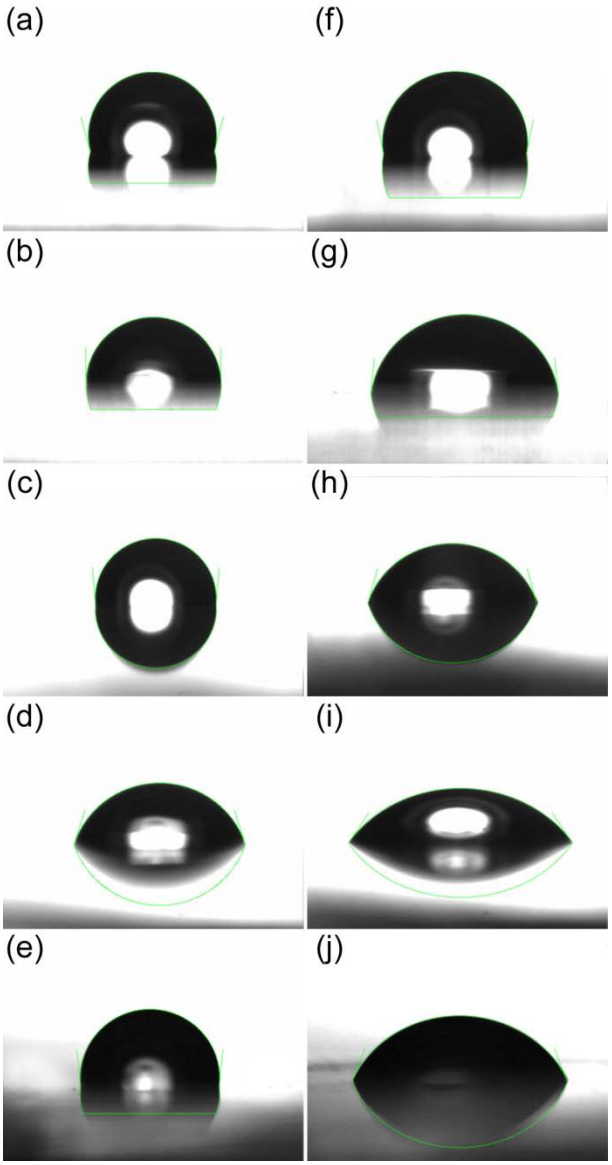

Figure 4.1 The images of contact angle measurement. (a–e) DI water drops on (a) bare PDMS, (b) UV-ozone treated PDMS, (c) polyethylene sulfonate (PES), (d) PES/graphene and (e) PDMS/graphene. (f–j) Ethylene glycol drops on (f) bare PDMS, (g) UV-ozone treated PDMS, (h) PES, (i) PES/graphene and (j) PDMS/graphene.

Table 4.1 Measured contact angles and calculated surface energy values.

Surface	DI water (°)	Ethylene glycol (°)	γ^d (mJ m^{-2})	γ^p (mJ m^{-2})	γ (mJ m^{-2})
Bare PDMS	108.0±2.7	100.5±1.3	0.7	1.5	2.2
UV-ozone treated PDMS	87.5±2.7	84.7±0.5	0.3	5.4	5.7
PES	95.7±1.0	77.0±2.3	3.5	1.1	4.6
PES/graphene	72.2±0.4	55.9±0.5	2.7	5.0	7.8
PDMS/Graphene	95.8±0.8	67.3±1.8	7.2	0.2	7.4

Note: γ, surface energy; *d*, dispersion component; *p*, polar component.

The sheet resistance change of graphene films before and after transferring is shown in Figure 4.2. The sheet resistance of PES / graphene before transferring was 268±25 Ω $\square^{-1}$ and that of PDMS / graphene after transferring on PDMS was 803±166 Ω $\square^{-1}$, indicating reduced conductance of graphene after transferring might be attributed to incomplete transfer of graphene films.

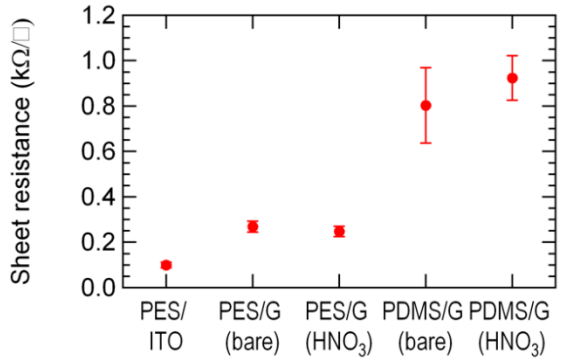

Figure 4.2 Sheet resistance of ITO and graphene films. The sheet resistance values were measured at different 10 regions and averaged (bars show one standard deviation).

The wet doping agent of 2 ml HNO_3 (63%) was dropped on the bottom of a petri dish. The PDMS / graphene substrates were attached to the top of the petri dish lid. During closure of the petri dish for 2 min, HNO_3 vapor was exposed to graphene electrodes. After *p*-doping, graphene / PDMS substrates were dried for 10 min under ambient condition. The detailed effect of HNO_3-doping was described in the previous report [42].

When graphene was *p*-doped, the work function value was lowered by 0.04 eV from 4.87 eV (non-doped) to 4.91 eV (*p*-doped), as shown in Figure 4.3.

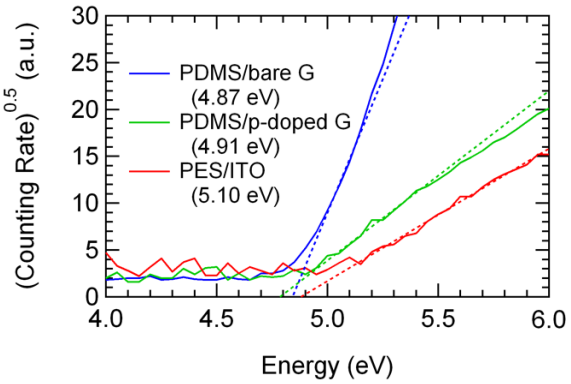

Figure 4.3 Photoelectron emission spectra of non-doped and p-doped graphene films on PDMS for anode and PES / ITO for cathode.

4.1.2 Optimization of hole injection from graphene anodes

To conform the role of MoO_3 as a hole injection layer, we compared the two structures of ITO / ZnO / green QDs / CBP / MoO_3 / graphene and ITO / ZnO / green QDs / CBP / graphene. Graphene electrodes were *p*-doped with nitric acid (HNO_3) as a *p*-doping agent. Comparing to the device with MoO_3, the device without MoO_3 showed very low current density and almost no light intensity, which are attributed to the disability of the hole injection from the graphene electrode to CBP (Figure 4.4(a) and (b)).

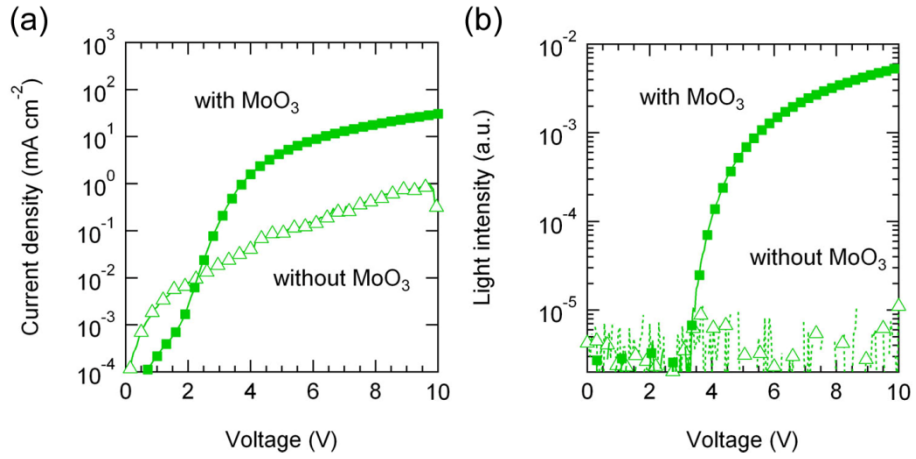

Figure 4.4 (a), Current density–voltage characteristics. The device with MoO_3 (close squares) showed larger current density at the same voltages than the one without MoO_3 (open triangles). (b) Light intensity–voltage characteristics. The device with MoO_3 (close squares) was normally turned on as current density increased, however, the one without MoO_3 (open triangles) did not emit light.

The wet doping agent of 2 mL HNO_3 (63%) was dropped on the bottom of a petri dish. The graphene/PDMS substrates were attached to the top of the petri dish and the cover was closed for 2 min. After *p*-doping with HNO_3 vapor in the closed petri dish, PDMS / graphene substrates were dried for 10 min under ambient condition. The detailed effect of *p*-doping with HNO_3 on a graphene film was investigated in the previous report [42]. The green TFQLED using a *p*-doped graphene electrode showed higher current density and brightness than that using non-doped one (Figure 4.5(a) and (b)). Also, efficiencies were 2-fold higher in the *p*-doped graphene device than in the non-doped graphene device.

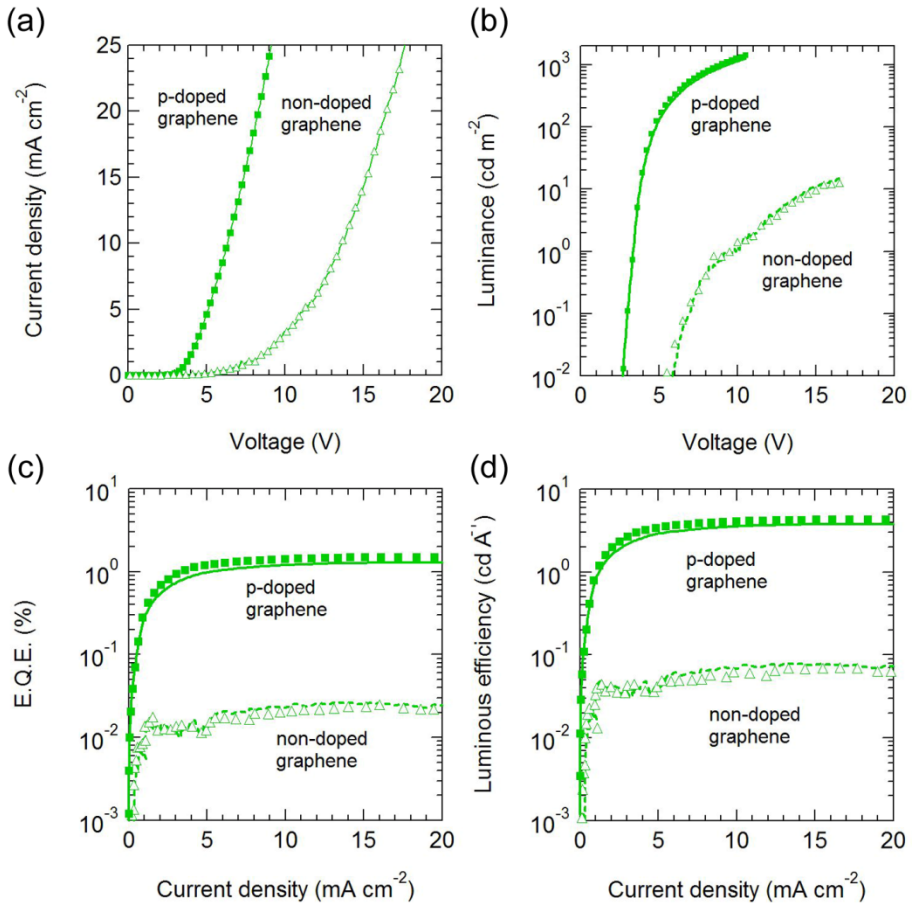

Figure 4.5 (a) Current density–voltage characteristics. The *p*-doped device (close squares) showed larger current density at the same voltages than the non-doped one (open triangles). (b) Luminance-voltage, (c) external quantum efficiency (EQE)– and (d) luminous efficiency (LE)–current density characteristics. Luminance, EQE and LE values were two orders higher in the *p*-doped device than in the non-doped one.

4.1.3 Device structure and fabrication

A schematic procedure of graphene lamination and the device structure are shown in Figure 4.6(a). Based on the previous work [25,60], we chose an inverted device structure because of superior carrier injection into the QDs, selectivity of various HTLs possessing low the highest occupied molecular orbital (HOMO) energy levels and resultant energy level alignment as shown in Figure 4.6(b). The device construction begins with a patterned ITO cathode on a PES substrate (~200 μm). Upon that substrate, a 50-nm-thick ZnO nanoparticle film serving as an electron injection layer (EIL) and electron transport layer (ETL) was spin-coated. The emission layer is composed of a 20-nm-thick layer of QDs, followed by a 40-nm-thick CBP layer for HTL and 10-nm-thick MoO_3 layer for HIL. Finally, a pre-patterned graphene anode attached to a thin PDMS substrate (~500 μm) is laminated on top of the device.

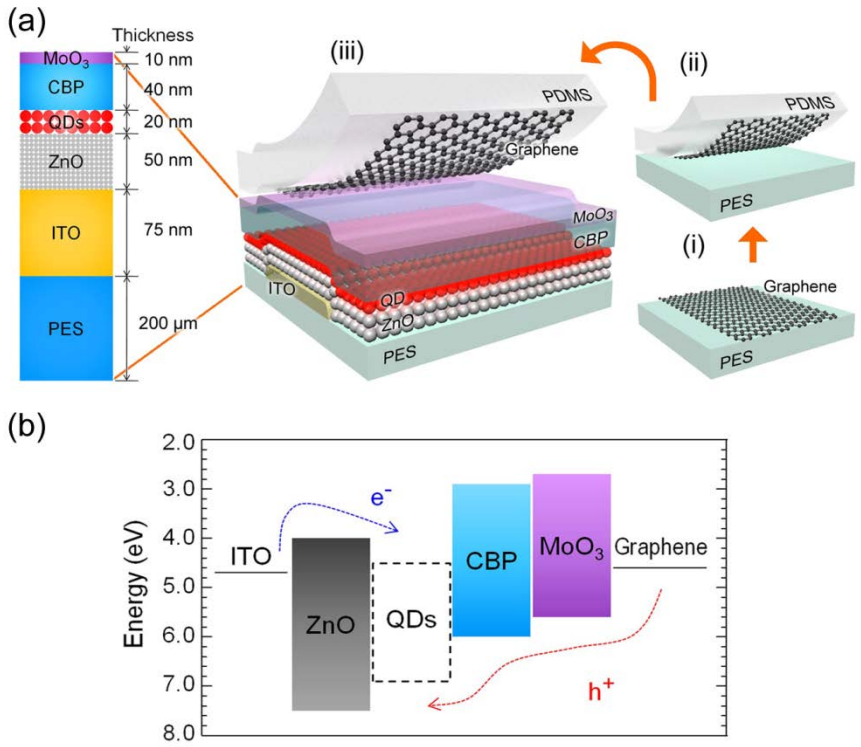

Figure 4.6 (a) Patterned graphene sheets on PES substrate (i) were transferred to UV-ozone treated PDMS substrate by soft-contact and peel-off method due to the difference of work of adhesion (ii), followed by attaching PDMS / graphene substrate as an anode on the top of the device deposited in the sequence of ITO (as a cathode), ZnO, QDs, CBP and MoO_3 on the PES substrate (iii). (b) Energy level diagram of semiconducting materials composing the TFQLED.

4.1.4 Electroluminescence Characteristics

The current–voltage and luminance–voltage characteristics of red, green and blue TFQLEDs are shown in Fig. 4.7(a) and (b). Because the hole injection barrier between CBP and QDs is different depending on the QD color, the driving voltages of each device at the same current density increases with increasing QD band gap. The turn-on voltages of each TFQLED are as low as 1.9 V for red, 2.7 V for green and 3.1 V for blue QDs, which values are mainly determined by the difference in the hole injection barrier between the HOMO energy level of CBP and the valence band level of different color quantum dots. Herein, it is noticeable that the turn-on voltages are close to the band gap of each quantum dot, which means that MoO_3/graphene doped as *p*-type made nearly ohmic contact. A few papers using graphene as an anode have been reported previously [39,40], but they showed plain performances especially on their turn-on voltages. We attribute these improvements to using MoO_3 as an HIL and *p*-doped graphene as an anode.

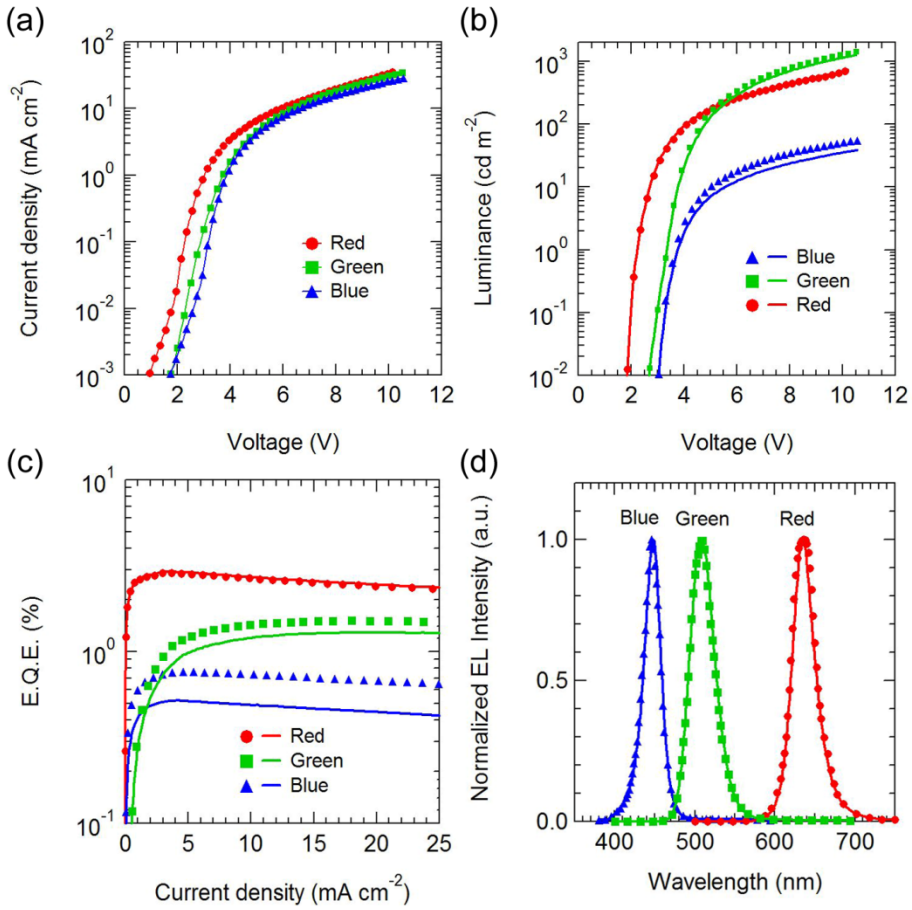

Figure 4.7 (a) Current density–voltage characteristics of red (circles), green (squares) and blue (triangles) TFQLEDs. (b) Luminance–voltage, (c) external quantum efficiency–current density characteristics and (d) electroluminescence (EL) spectra of TFQLEDs measured through both graphene (circles, squares, and triangles) and ITO (red, green and blue lines) for red, green and blue devices, respectively. The EL spectra were measured at the current density of 5 mA cm^{-2}. Device performances were much higher through the graphene than ITO without any change in their spectral shapes. a.u., arbitrary units.

The luminance was measured from both the ITO and graphene sides as shown in Fig. 4.7(b). Measuring through the ITO side, the maximum luminances were 700, 1,250 and 40 cd m^{-2}, for the red, green, and blue emitting devices at the driving voltage of 10.1, 10.5 and 10.6 V, respectively. Measuring through the graphene side, on the other hand, the luminances were 690, 1,430 and 60 cd m^{-2}, for the red, green, and blue emitting devices, respectively. Similarly, measuring EQE through the ITO side yields 2.9, 1.3 and 0.5% while measuring through the graphene side yields 2.9, 1.5 and 0.8%, for the red, green and blue emitting devices, respectively (Fig. 4.7(c)). Examining the difference of the luminance and EQE values pursuant to the direction of measurement, the luminance and EQE are significantly larger (i.e., ~15% for the green device and ~45% for the blue device) measured through the graphene side compared to those measured through the ITO. For the red device, the difference is negligible. EL spectra measured at 5 mA cm^{-2} also show no difference by the measuring direction as shown in Fig. 4.7(d). Device performances of red, green and blue TFQLEDs are summarized in Table 4.2. Figure 4.8(a–f) shows the photographs of red, green and blue TFQLEDs showing their transparency and flexibility.

Table 4.2 Summary of the device performances of TFQLEDs

Emissive side	Color	Max. EQE (%)	Max. luminance (cd m^{-2})	EL λ_{max} (nm)	CIE index (x, y)	T at EL λ_{max} (%)
Red	ITO	2.9	700	635	(0.70, 0.30)	74.8
	Graphene	2.9	690	637	(0.70, 0.30)	
Green	ITO	1.3	1,250	507	(0.11, 0.65)	67.0
	Graphene	1.5	1,430	509	(0.10, 0.65)	
Blue	ITO	0.5	40	448	(0.16, 0.03)	63.1
	Graphene	0.8	60	446	(0.16, 0.03)	

Note: EQE, the maximum external quantum efficiency; LE, luminous efficiency; λ_{max}, EL peak wavelength; CIE, Commission Internationale de l'Eclairage.

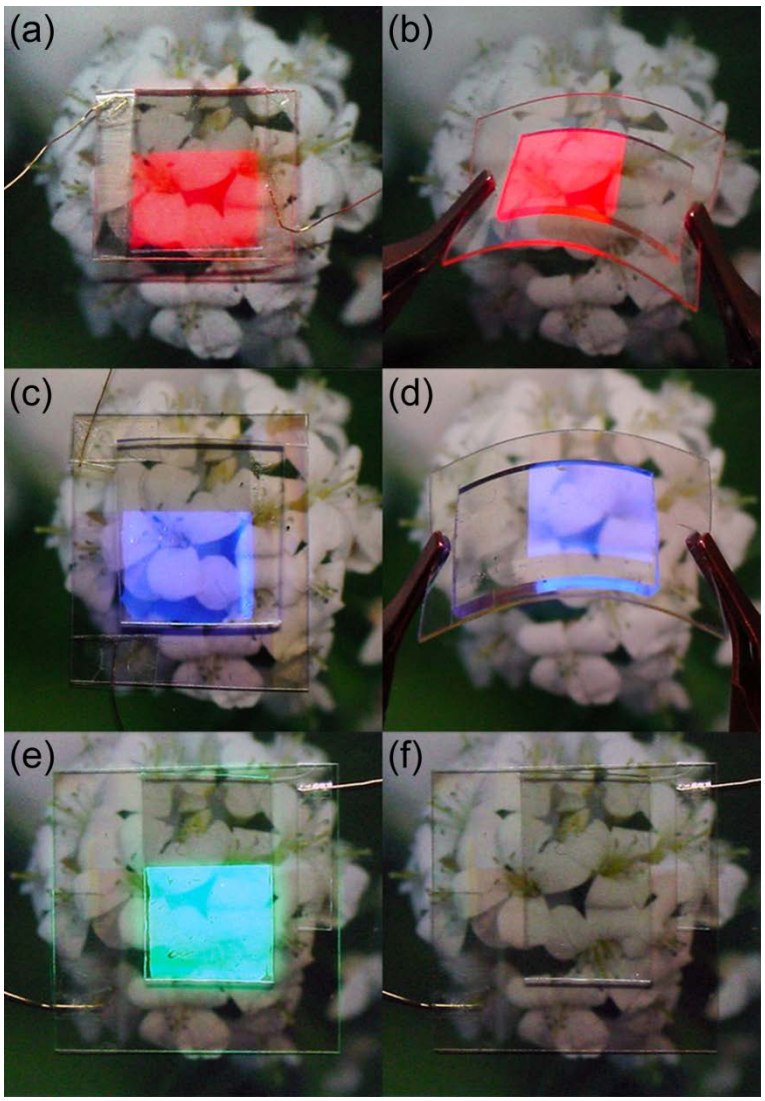

Figure 4.8 Photographs of (a,b) red, (c,d) blue and (e,f) green emission from flat and bent TFQLEDs. The active area of each device is 5 mm × 7 mm. Turned-off device shows the background image clearly owing to the high transparency of TFQLED.

4.1.5 Transmittance and reflectance characteristics

The considerable increase in luminance and EQE when measuring through the graphene side can be attributed to both the better transmission and lower reflectivity of graphene as compared to ITO as plotted in Figure 4.9. In addition, photons created in the emission layer traveling towards and then reflected by the ITO further increase the luminance and EQE measured through the graphene side. Since the transmission of graphene and ITO are similar in the red portion of the spectrum, the values for luminance and EQE are closer in this region. These results are particularly important because blue emitting materials are significantly less efficient compared to green or red emitting materials. Therefore, the increase in transmission and reduction in reflectivity obtained by using graphene is a great advantage.

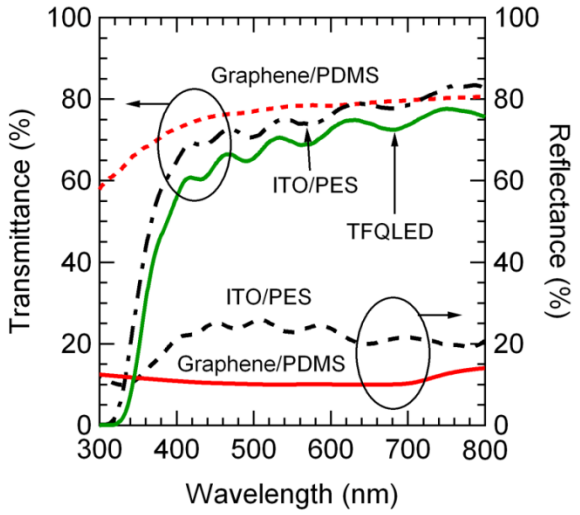

Figure 4.9 Graphene / PDMS (red dot line) is more transparent in entire visible range compared to ITO / PES (black dash-dot line) and the reflectance of graphene / PDMS (red line) is smaller than ITO / PES (black dash line), so the device showed better performances through graphene than through ITO. The transmittance of a complete green TFQLED device (green thick line) is also plotted to display the transmittance of turn-off state.

4.1.6 Angular dependent EL characteristics

As shown in the angular emission characteristics in Fig. 4.10(a–c), there is little evidence of the microcavity effect in our TFQLEDs. The peak wavelength of the EL emission in the green device, for example, shifted only by 1 nm, that is, from 511 nm at normal direction to 512 nm at 80° off the

normal direction (see Figure 4.10(a) and (b)). The full width at half maximum (FWHM) also changed by only 2 nm (from 35 nm at normal direction to 37 nm at 80° off the normal direction), which are significantly smaller values compared to other top-emitting devices. Typically in top-emitting devices, the shift of EL peak wavelength as well as the changes of FWHM are big issues because they results changes in color coordinate, color temperature and color rendering index as well [38,61]. The reduction in peak shift and FWHM change can be explained due to the significant reduction in reflectivity of graphene vs. a second ITO or other reflective metal layer. These results indicate that a graphene top electrode could be useful for other optoelectronic devices in order to reduce the changes in the peak wavelength of EL emission and their FWHM. The (square symbols) emission profile and (line) Lambertian profile are also nearly identical for each side as shown in Figure 4.10(c), so this device structure is applicable to display devices.

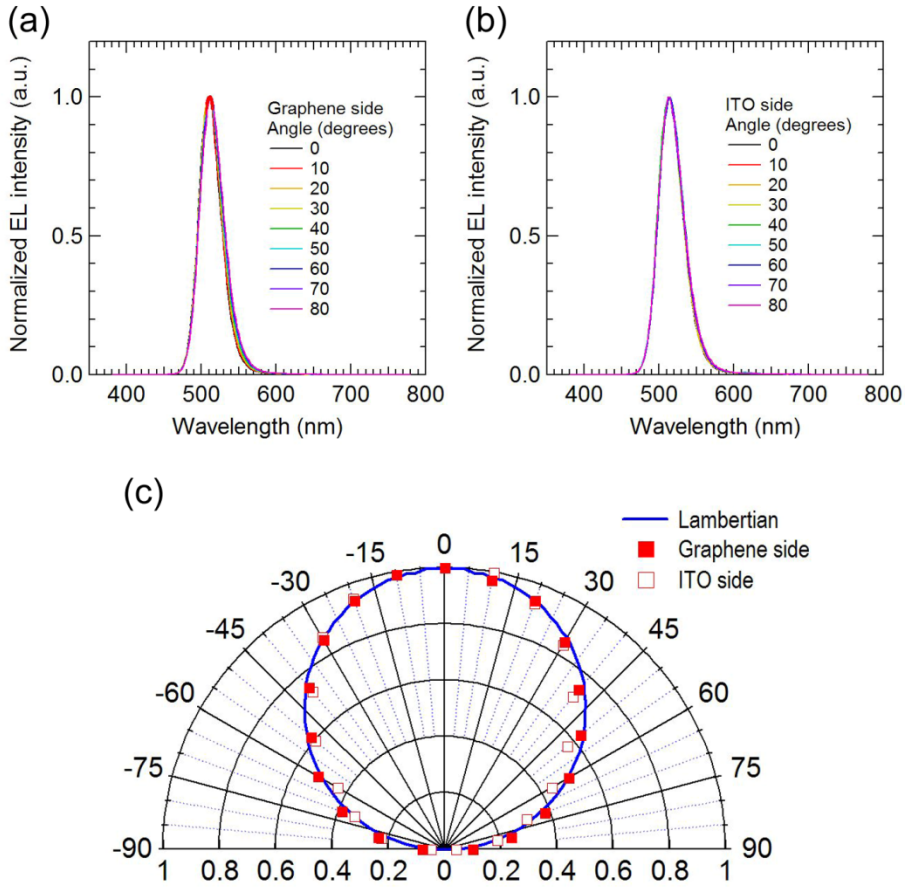

Figure 4.10 Angular dependent EL spectra of top emission through (a) graphene and (b) ITO electrodes. The changes in the peak wavelength and FWHM of the emission through graphene as a function of EL measuring are very small by 1–2 nm. (c) The angular emission profiles of (open squares) ITO-side and (close squares) graphene-side were compared with (line) Lambertian profile.

4.1.7 EL characteristics under bending conditions

With a green TFQLED, EL characteristics were measured under bending and unbending conditions. As you can see in the Figure 4.11(a), the change of EL spectra was small when the device was on bending. As shown in Figure 4.11(b), the efficiencies on bending from 0.24% strain (bending radius (R) = 102 mm) to 7.5% strain (R = 3.69 mm) did not changed much (~1.2%). When the strain went over 7.5% (R < 3.69 mm), the efficiency decreased rapidly to 0.2%. This might be the crack formation in ITO electrode. The EQE was measured until 10.8% strain (R = 2.67 mm), then at strain > 10.8%, the device was broken.

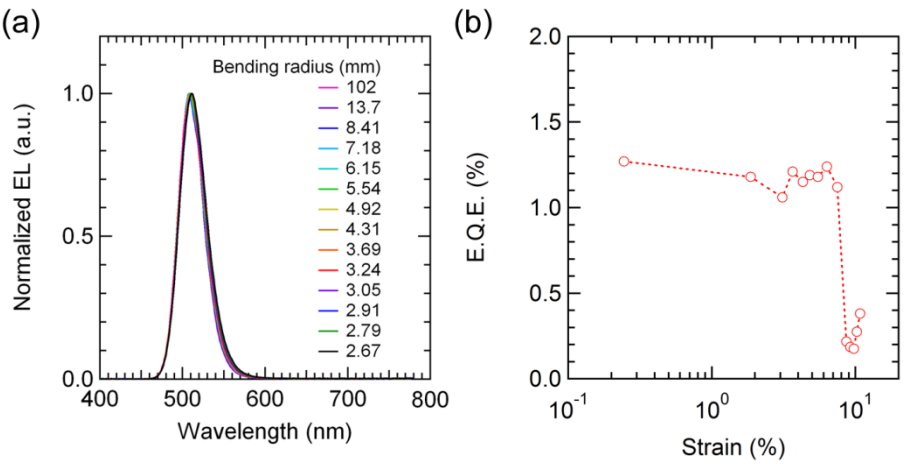

Figure 4.11 (a) EL spectra and (b) external quantum efficiency as a function of strain under bending and unbending conditions

4.1.8 Lifetime characteristics

The operating lifetime of TFQLEDs using graphene sheets as a top anode was compared with that of conventional flexible QLEDs (PES / ITO / ZnO / QDs / CBP / MoO_3 / Al) for red, green and blue devices. The graphene devices were operated at constant current density (red: 12.2, green: 9.2, blue: 12.2 mA cm^{-2}) and also the Al devices were operated at constant current density (red: 14.4, green: 9.7, blue: 19.1 mA cm^{-2}). For the red, green and blue devices, the current density values corresponded to the luminance values of 500, 500 and 50 cd m^{-2}, respectively. The normalized luminance–time characteristics of all devices were plotted in Figure 4.12. The operating lifetime data were recorded using a McScience Polaronix^{TM} OLED Lifetime Test System. The half luminance lifetime values of TFQLEDs using graphene anode were shorter (red: 21, green: 1.6, blue: 0.46 hours), compared to those of QLEDs using Al anode (red: 290, green: 3.9, blue: 0.56 hours).

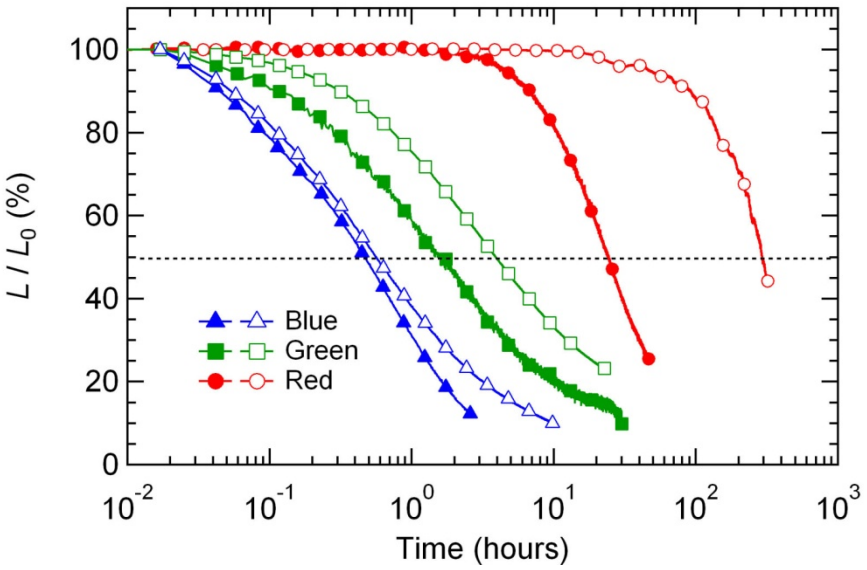

Figure 4.12 The operating lifetime of red, green and blue QLEDs with graphene and Al electrodes as an anode. (close markers) Graphene devices were compared with (open markers) Al devices. The (circles) red, (squares) green and (triangles) blue devices were operated at the constant current which corresponded to initial luminances (L_0) of 500, 500, and 50 cd m^{-2}.

4.2 Highly Transparent and Flexible QLEDs Using Graphene Electrodes as Both Anode and Cathode

4.2.1 Optimization of electron injection from graphene cathodes

To improve transparency and flexibility of the above TFQLED which has the device structure of ITO / ZnO / QDs / CBP / MoO_3 / Graphene, it is needed to replace a conventional metal oxide cathode of ITO with more unbreakable and transparent electrode. Because graphene electrodes worked well as an anode in the previous section (Chap. 4.2). We used the graphene electrode as a substitute for ITO anode. However, electron injection from graphene cathode to ZnO was not proved yet. In the previous study, electron transport from ZnO nanoparticles to graphene oxide was observed [62]. UV-ozone treatment is able to generate graphene oxide on top of a graphene film. As a sort of solution to inject electron efficiently from graphene cathodes, UV-ozone treatment was performed on graphene films.

To verify the effect of UV-ozone treatment, Raman spectroscopy was performed with monolayer graphene films on Si / SiO_2 substrates by changing the UV-ozone treatment duration as shown in Figure 4.13(a) and (b). The two intense peaks are the G peak at ~1,580 cm^{-1} and the 2D peak at ~2,700 cm^{-1} [63]. The other peak at ~1,350 cm^{-1} is the defect-related D peak. In Raman spectra for 10 min and 20 min UV-ozone-treated samples, the intensity peaks diminished indicating that monolayer graphene film was removed after 10

min UV-ozone treatment (see Figure 4.13(a)). From 1 min to 4 min, G peak was maintained while D peak was increased indicating that the main structure of graphene film was sustained while defects including graphene oxide were generated (see Figure 4.13(b)).

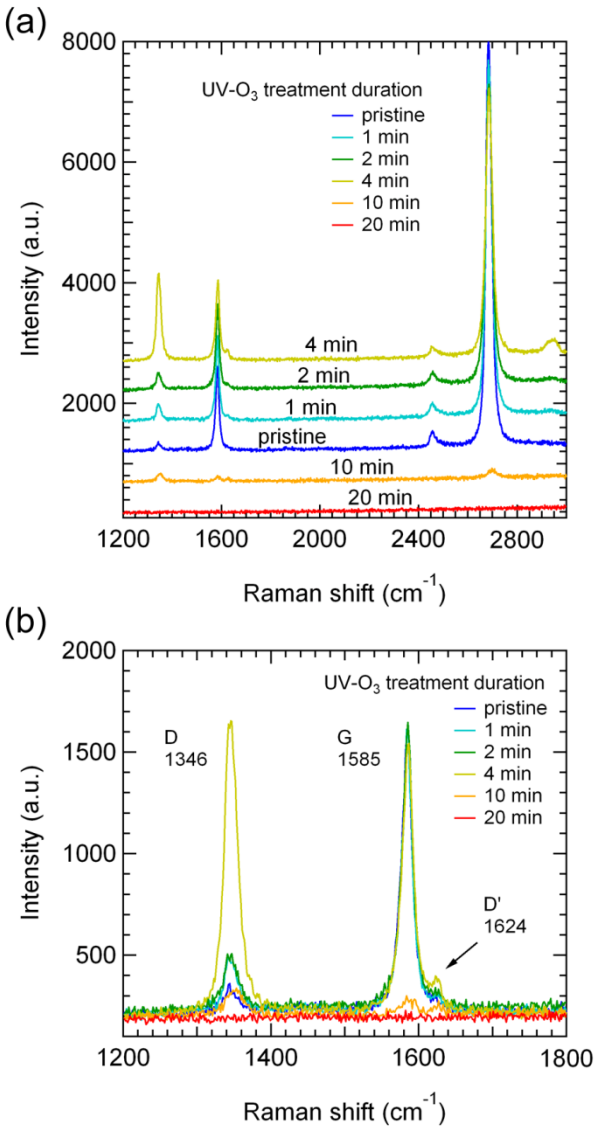

Figure 4.13 (a,b) Raman spectra of monolayer graphene films with increasing UV-ozone treatment duration

Also, we check the change of the sheet resistance as a function of UV-ozone treatment duration. The sheet resistances of the bare film showed 216±8 Ω □$^{-1}$ and those of the 1-min, 2-min and 4-min UV-ozone treated films had slightly higher values of 241±23, 252±13 and 260±18 Ω □$^{-1}$ than that of bare film. For the 10-min and 20-min treated films, the sheet resistance values increased by 1.9 times and 4.6 times compared to the bare film. It is corresponding to Raman spectra of the 10-min and 20-min treated films (see Figure 4.14).

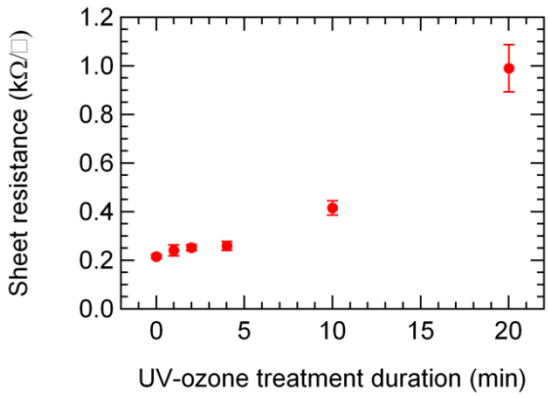

Figure 4.14 Sheet resistance of PET / graphene films with the different UV-ozone treatment duration. The sheet resistance values were measured at different 10 regions and averaged (bars show one standard deviation).

By using photoelectron emission spectroscopy, work function values were measured. When we increased UV-ozone treatment duration, the work function values decreased from 4.88 eV (bare graphene) to 4.85 eV (20 min UV-ozone treated graphene). Lowering the work function value of graphene can help the electron injection to ZnO ETL.

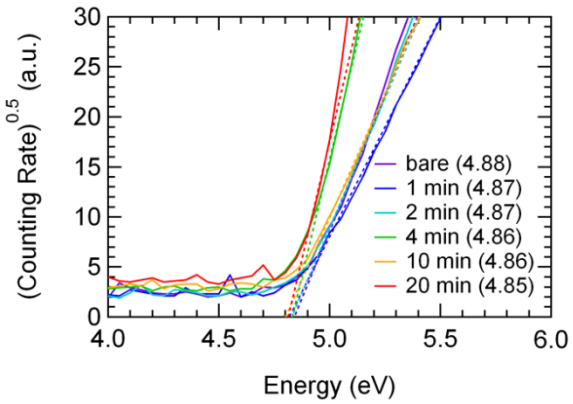

Figure 4.15 Photoelectron emission spectra of PET/graphene films with the different UV-ozone treatment duration. Figures in parenthesis refer to the work function values of various graphene films.

The morphology of ZnO-coated graphene film was characterized by AFM (see Figure 4.16). By increasing UV-ozone treatment duration from non-treated to 4 min, the morphology changed rougher. The mean roughness values of bare, 1-, 2- and 4-min samples were 4.8, 6.3, 7.4 and 9.2 nm, respectively. For the 10-min and 20-min treated samples, the mean roughness decreased and the values were 6.4 and 4.5 nm, respectively. However, few

large dots were observed. Their diameter and height were over 0.5 μm and 60 nm, respectively.

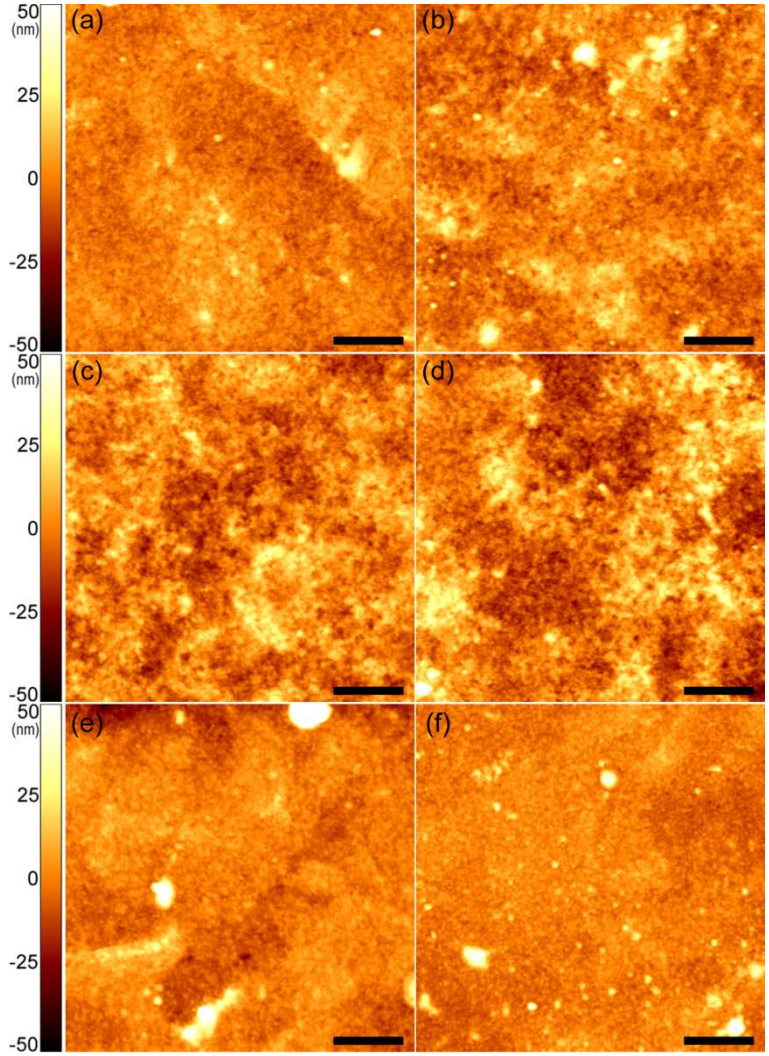

Figure 4.16 AFM images of ZnO-coated graphene films. Graphene films were (a) bare and UV-ozone treated for (b) 1 min, (c) 2 min, (d) 4 min, (e) 10 min and (f) 20 min. Scale bars represent 2 μm.

However, the morphologies at the different location may not the correct comparison. The morphology changes were also investigated by taking the AFM images at the same location with increasing UV-ozone treatment time. For 4 min of UV-ozone treatment, the morphology of graphene film did not change (see Figure 4.17(a-d)). The mean roughness values of non-treated film and 1-, 2-, and 4-min UV-ozone treated films were 2.9-3.0 nm.

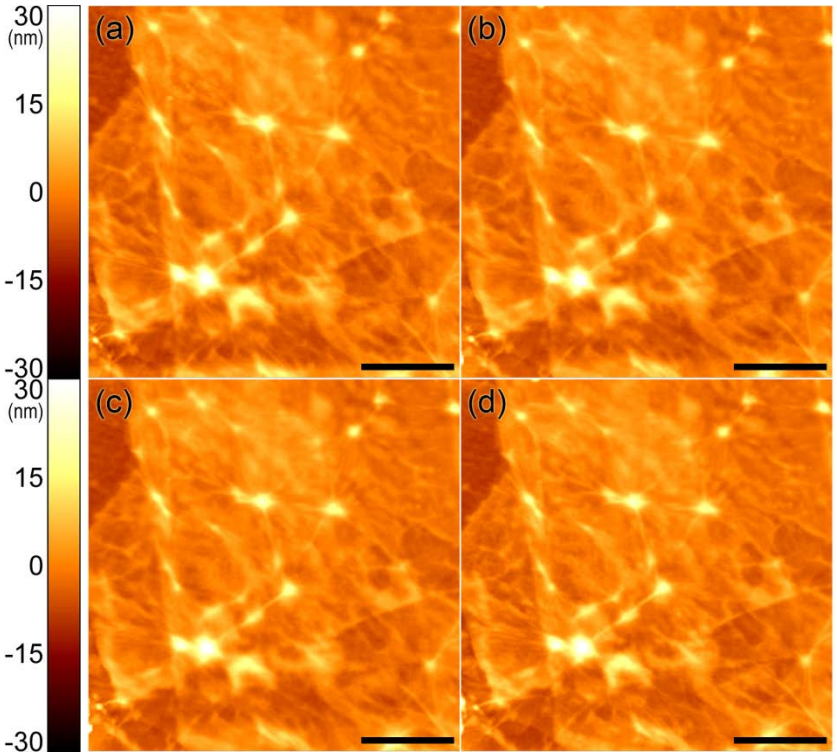

Figure 4.17 AFM images of graphene films. Graphene films were (a) bare and UV-ozone treated for (b) 1 min, (c) 2 min, (d) 4 min. Scale bars represent 1 μm.

To compare the injection properties of bare graphene and UV-ozone treated graphene to ZnO ETL layer, we compare the blue TFQLED devices with the different cathodes of bare graphene, UV-ozone treated graphene, *p*-doped graphene and ITO. The device structure was cathode (graphene or ITO) / ZnO (50 nm) / blue QDs / CBP (60 nm) / MoO_3 (10 nm) / p-doped graphene / PDMS. Device characteristics are shown in Figure 4.18(a–d). In Figure 4.17(a), the leakage current density of UV-ozone treated one at the low voltage region from 0 to 4 V was lower than p-doped and bare ones. *P*-doped graphene showed the highest leakage indicates that even at low bias voltage the hole current flows easily from the anode (*p*-doped graphene) to the cathode (*p*-doped graphene) probably having the same work function with the anode. The values of luminance and efficiency were also high in the order of UV-ozone treated, bare and *p*-doped graphene devices. The maximum total luminance values of top and bottom side were 65, 40 and 2 cd m^{-2} and the maximum total luminous efficiency values were 0.27, 0.11 and 0.006 cd A^{-1} corresponding to the maximum total external quantum efficiency values of 1.3, 0.37 and 0.015 % for UV-ozone treated, bare and *p*-doped graphene devices, respectively.

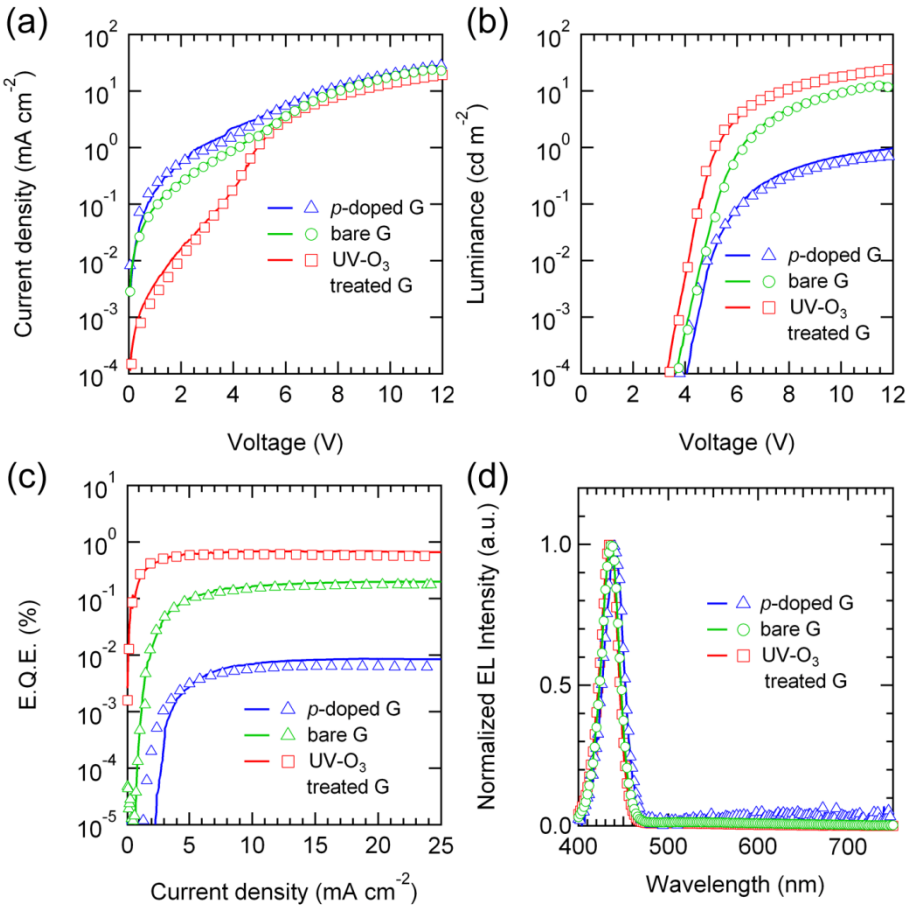

Figure 4.18 (a) Current density–voltage characteristics, (b) Luminance-voltage, (c) external quantum efficiency (EQE)– and (d) luminous efficiency (LE)–current density characteristics of blue TFQLEDs with the different cathodes of bare graphene, UV-ozone treated graphene, *p*-doped graphene and ITO electrodes and the *p*-doped graphene.

4.2.2 Electroluminescence characteristics

As a similar way, the red, green and blue TFQLEDs using graphene electrodes as an anode and a cathode were fabricated with the above optimized condition. The current–voltage and luminance–voltage characteristics of red, green and blue TFQLEDs are shown in Figure 4.19(a) and (b). Because the hole injection barrier between CBP and QDs is different depending on the QD color, the driving voltages of each device at the same current density increases with increasing QD band gap. The turn-on voltages of each TFQLED are as low as 1.9 V for red, 2.7 V for green and 3.1 V for blue QDs, which values are mainly determined by the difference in the hole injection barrier between the HOMO energy level of CBP and the valence band level of different color quantum dots. The key performances of RGB TFQLEDs were summarized in Table 4.3. These TFQLEDs using graphene electrodes as both cathode and anode showed almost identical light emission through top and bottom directions while the TFQLEDs using ITO cathode and graphene anode showed larger light intensity through graphene direction than that through ITO direction at the blue–green region. EQEs were plotted in Figure 4.19(c). Maximum EQE values were 2.9, 1.2 and 0.7% through bottom direction (PET/graphene) and 2.8, 1.2 and 0.6% through top direction (graphene/PDMS), for the red, green and blue TFQLEDs, respectively. The peak wavelengths of EL spectra were also similar through both directions and 636, 523 and 435 nm, for the red, green and blue devices, respectively (see Figure 4.18(d)). It is noteworthy that the transmittance of TFQLEDs reached

over 70% even at the peak wavelength of blue EL spectrum. The CIE color coordinates were (0.70, 0.30), (0.19, 0.71) and (0.17, 0.03) for the red, green and blue ones. It indicates that the color gamut of these TFQLEDs reached 112% of NTSC 1953 color space.

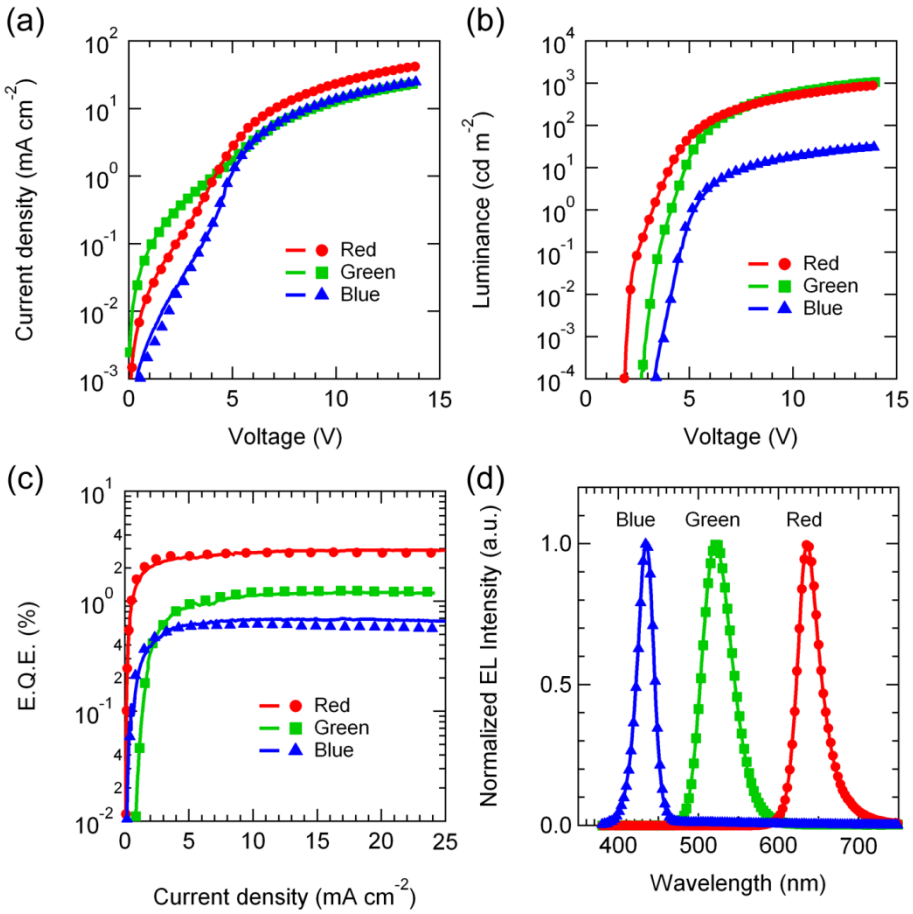

Figure 4.19 (a) Current density–voltage characteristics of red (circles), green (squares) and blue (triangles) TFQLEDs. (b) Luminance–voltage, (c) external quantum efficiency–current density characteristics and (d) electroluminescence (EL) spectra of TFQLEDs measured through both graphene (circles, squares, and triangles) and ITO (red, green and blue lines) for red, green and blue devices, respectively. The EL spectra were measured at the current density of 5 mA cm^{-2}.

Table 4.3 Summary of the device performances of TFQLEDs using graphene electrode as an anode and a cathodes.

Color	Emissive side	Max. EQE (%)	Max. luminance (cd m^{-2})	EL λ_{max} (nm)	CIE index (x, y)	T at EL λ_{max} (%)
Red	Bottom	2.9	970	636	(0.70, 0.29)	75.9
	Top	2.8	900	636	(0.70, 0.30)	
Green	Bottom	1.2	1,050	521	(0.19, 0.71)	74.9
	Top	1.2	1,070	523	(0.19, 0.71)	
Blue	Bottom	0.7	34	435	(0.17, 0.03)	70.1
	Top	0.6	31	435	(0.17, 0.03)	

Figure 4.20(a-i) shows the photographs of RGB TFQLED devices when they were flat off, flat on and bent on. In the Figure 4.20(a), (d) and (g), back ground flower images were visible through RGB devices due to their high transmittance.

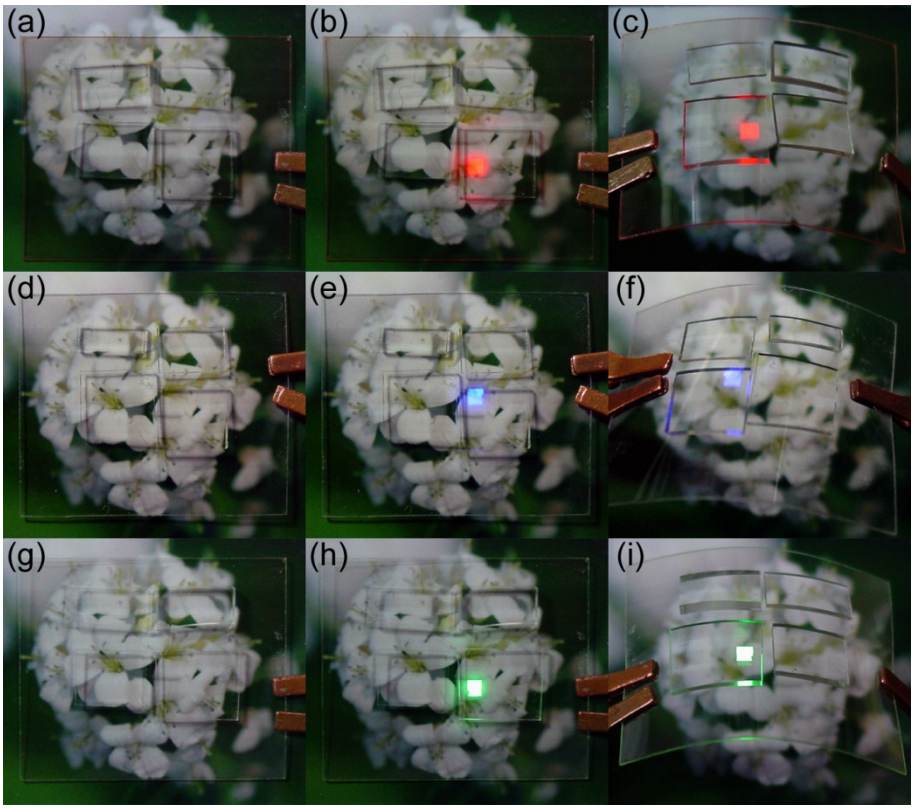

Figure 4.20 Photographs of (a–c) red, (d–f) blue and (g–i) green emission from flat off, flat on and bent on TFQLEDs. Turned-off device shows the background image clearly owing to the high transparency of TFQLED. The emission area of each device was 1.4 mm × 1.4 mm.

4.2.3 Transmittance characteristics

Transmittance characteristics were plotted in Figure 4.21. The complete TFQLED device using graphene/graphene (cathode/anode) showed higher average transmittance of 74.5% than that of the TFQLED device using ITO / graphene (70.8%).

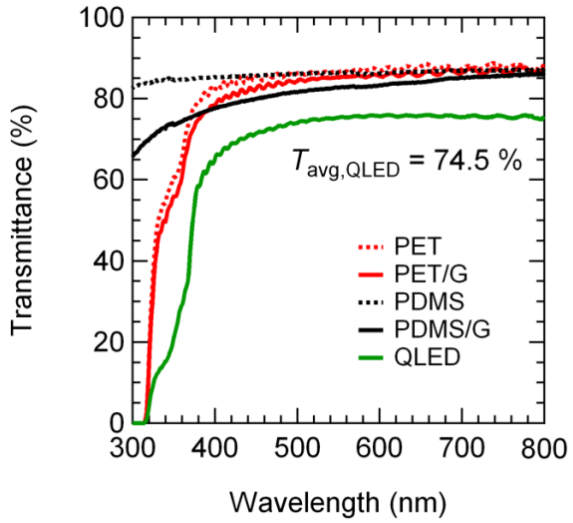

Figure 4.21 Transmittance characteristics of (red dashed) PET, (red solid) PET/graphene, (black dashed) PDMS, (black solid) PDMS/graphene. The transmittance of a complete TFQLED device using graphene as an anode and a cathode (green solid line) is also plotted to display the transmittance of turn-off state.

4.2.4 EL characteristics under bending conditions

With a red TFQLED, EL characteristics were measured under bending and unbending conditions. As you can see in the Figure 4.22(a), the change of EL spectra was small when the device was on bending and unbending. The efficiencies on bending from 0.51% strain (bending radius (R) = 19.5 mm) to 1.9% strain (R = 5.3 mm) did not changed much (see Figure 4.22(b)). When strain went over 1.9 % (R < 5.3 mm), the efficiency decreased until 7.3% strain (R = 1.4 mm) from 2.55% at 1.9% strain to 1.51% at 7.3% strain. The device efficiency was not recovered under unbending condition. After measurements were done, the efficiency changed from 2.26% to 1.20%.

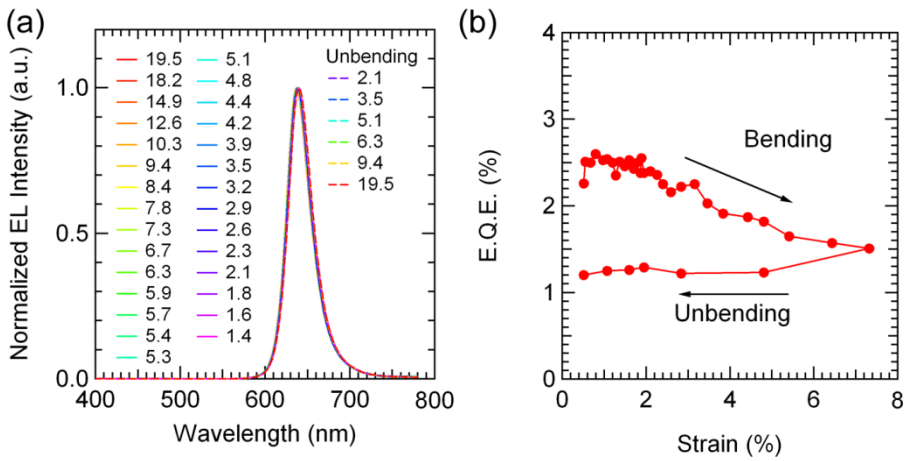

Figure 4.22 (a) EL spectra and (b) external quantum efficiency as a function of strain under bending and unbending conditions

4.2.5 Lifetime characteristics of TFQLEDs

The normalized luminance–time characteristics of red, green and blue TFQLEDs using graphene electrodes were plotted in Figure 4.23.

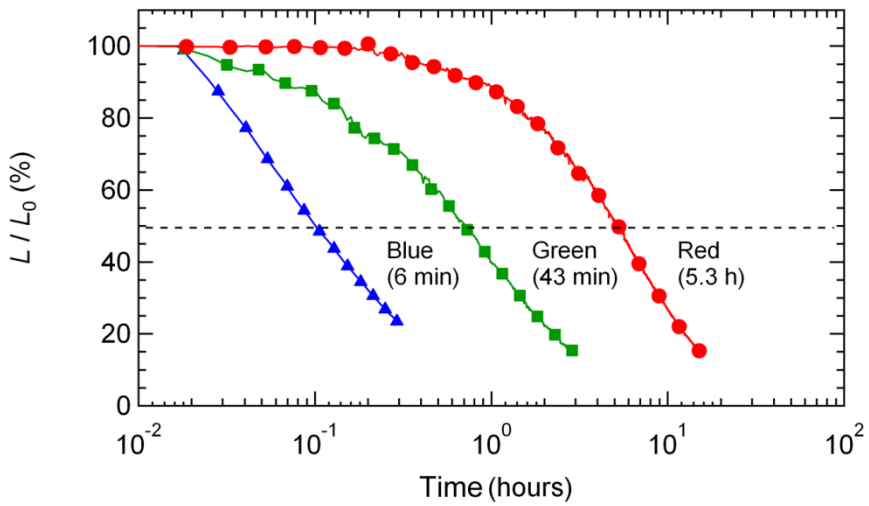

Figure 4.23 The operating lifetime of red, green and blue QLEDs with graphene as an anode and cathode. The (circles) red, (squares) green and (triangles) blue devices were operated at the constant current which corresponded to initial luminances (L_0) of 500, 500 and 50 cd m^{-2}.

For comparison, the QLED devices using graphene/graphene, ITO/graphene and ITO/aluminum (cathode/anode) were summarized in Table 4.4. When metal or metal oxide electrodes were replaced with graphene electrode, the lifetime of QLED devices seemed to get shorter which might be

attributed to increased oxygen and moisture penetration due to the defect of graphene films.

Table 4.4 Summary of half luminance lifetime of red, green and blue QLEDs with different electrode combinations

Color	graphene/graphene	ITO/graphene	ITO/Al
Red	5.3 h	21 h	290 h
Green	0.17 h	1.6 h	3.9 h
Blue	0.10 h	0.46 h	0.56 h

Chapter 5. Conclusion

In this thesis, high-performance colloidal quantum-dot light-emitting diodes have been studied in the view point of fabrication process and device structure. We developed and demonstrated highly transparent and flexible quantum-dot light-emitting diodes with transparent electrodes.

First, the soft-contact transplanting technique was adopted to QLEDs and compared to the conventional spin coating technique. The red, green and blue QLEDs with transplanted QD layers showed comparable device performances to those with spin-coated QD layers. To improve device performance and suppress the parasitic emission due to vacancies, we tested various vacuum-deposited hole transporting materials as a top surface to transfer QD layers. Patternability differences of transplanted QD patterns on those HTLs were observed and investigated by means of fluorescence optical microscopy, surface energy calculation and electroluminescence characterization with green QLEDs.

The transfer technique was also applied to fabricating transparent and flexible QLEDs. Transparent and conductive graphene films on plastic substrate were transferred to PDMS surface which is able to make conformal contact. PDMS/graphene substrates were successively laminated on the device substrate and worked as an anode. For efficient hole injection from graphene anode, MoO_3 was adopted and graphene films were *p*-doped with nitric acid. The average transmittance of 70.8% was achieved with the

TFQLED structure of PES / ITO / ZnO / QDs / CBP / MoO_3 / *p*-doped graphene / PDMS. Additionally, angular dependence and lifetime were measured with three primary color QLEDs.

Finally, TFQLEDs using graphene films as both anode and cathode without an ITO electrode were fabricated by optimizing the electron injection property of graphene cathode to the electron transport layer. UV-ozone treatment for adequate duration time enhanced the efficient electron injection, however, UV-ozone treatment more than needed duration resulted in reduced conductivity of graphene films due to the top layer damage of the graphene multilayer. The average transmittance of this TFQLED with the structure of PET / UV-ozone treated graphene / ZnO / QDs / CBP / MoO_3 / p-doped graphene / PDMS showed the increased value of 74.5% compared to the TFQLED using ITO cathode and graphene anode.

We believe that the device design and the fabrication method can be utilized to realize the novel future display applications.

Bibliography

[1] V. L. Colvin, M. C. Schlamp and A. P. Alivisatos, *Nature* **370**, 354 (1994).

[2] S. Coe, W. K. Woo, M. G. Bawendi and V. Bulović, *Nature* **420**, 800 (2002).

[3] M. C. Schlamp, Xiaogang Peng and A. P. Alivisatos, *J. Appl. Phys.* **82**, 5837 (1997).

[4] H. Mattoussi, L. H. Radzilowski, B. O. Dabbousi, E. L. Thomas, M. G. Bawendi and M. F. Rubner, *J. Appl. Phys.* **83**, 7965 (1998).

[5] M. Gao, C. Lesser, S. Kirstein, H. Möhwald, A. L. Rogach and H. Weller, *J. Appl. Phys.* **87**, 2297 (2000).

[6] S. Coe-Sullivan, Wing-Keung Woo, J. S. Steckel, M. Bawendi and V. Bulović, *Org. Electron.* **4**, 123 (2003).

[7] S. Coe-Sullivan, J. S. Steckel, Wing-Keung Woo, M. Bawendi and V. Bulović, *Adv. Funct. Mater.* **15**, 1117 (2005).

[8] J. S. Steckel, P. Snee, S. Coe-Sullivan, J. P. Zimmer, J. E. Halpert, P. Anikeeva, L.-A. Kim, V. Bulović and M. G. Bawendi, *Angew. Chem., Int. Ed.* **45**, 5796 (2006).

[9] J. Zhao, J. A. Bardecker, A. M. Munro, M. S. Liu, Y. Niu, I-K. Ding, J. Luo, B. Chen, A. K.-Y. Jen and D. S. Ginger, *Nano Lett.* **6**, 463 (2006).

[10] P. O. Anikeeva, J. E. Halpert, M. G. Bawendi and V. Bulović, *Nano Lett.* **7**, 2196 (2007).

[11] Y.-H. Niu, A. M. Munro, Y.-J. Cheng, Y. Tian, M. S. Liu, J. Zhao, J. A. Bardecker, I. J.-L. Plante, D. S. Ginger and A. K. -Y. Jen, *Adv. Mater.* **19**, 3371 (2007).

[12] Q. Sun, Y. A. Wang, L. S. Li, D. Wang, T. Zhu, J. Xu, C. Yang and Y. Li, *Nature Photon.* **1**, 717 (2007).

[13] J. M. Caruge, J. E. Halpert, V. Wood, V. Bulović and M. G. Bawendi, *Nature Photon.* **2**, 247 (2008).

[14] A. Rizzo, M. Mazzeo, M. Palumbo, G. Lerario, S. D'Amone, R. Cingolani and G. Gigli, *Adv. Mater.* **20**, 1886 (2008).

[15] P. O. Anikeeva, C. F. Madigan, J. E. Halpert, M. G. Bawendi and V. Bulović, *Phys. Rev. Lett.* **78**, 085434 (2008).

[16] L. A. Kim, P. O. Anikeeva, S. A. Coe-Sullivan, J. S. Steckel, M. G. Bawendi and V. Bulović, *Nano Lett.* **8**, 4513 (2008).

[17] A. Rizzo, M. Mazzeo, M. Biasiucci, R. Cingolani and G. Gigli, *Small* **4**, 2143 (2008).

[18] W. K. Bae, J. Kwak, J. Lim, D. Lee, M. K. Nam, K. Char, C. Lee and S. Lee, *Nanotechnology* **20**, 075202 (2009).

[19] W. K. Bae, J. Kwak, J. W. Park, K. Char, C. Lee and S. Lee, *Adv. Mater.* **21**, 1690 (2009).

[20] K.-S. Cho, E. K. Lee, W.-J. Joo, E. Jang, T.-H. Kim, S. J. Lee, S.-J. Kwon, J. Y. Han, B.-K. Kim, B. L. Choi, and J. M. Kim, *Nature Photon.* **3**, 341 (2009).

[21] J. Kwak, W. K. Bae, M. Zorn, H. Woo, H. Yoon, J. Lim, S. W. Kang, S. Weber, H.-J. Butt, R. Zentel, S. Lee, K. Char and C. Lee, *Adv. Mater.* **21**, 5022 (2009).

[22] P. O. Anikeeva, J. E. Halpert, M. G. Bawendi and V. Bulović, *Nano Lett.* **9**, 2532 (2009).

[23] W. K. Bae, J. Kwak, J. Lim, D. Lee, M. K. Nam, K. Char, C. Lee and S. Lee, *Nano Lett.* **10**, 2368 (2010).

[24] L. Qian, Y. Zheng, J. Xue and P. H. Holloway, *Nature Photon.* **5**, 543 (2011).

[25] J. Kwak, W. K. Bae, D. Lee, I. Park, J. Lim, M. Park, H. Cho, H. Woo, D. Yoon, K. Char, S. Lee, and C. Lee, *Nano Lett.* **12**, 2362 (2012).

[26] T.-H. Kim, K.-S. Cho, E. K. Lee, S. J. Lee, J. Chae, J. W. Kim, D. H. Kim, J.-Y. Kwon, G. Amaratunga, S. Y. Lee, B. L. Choi, Y. Kuk, J. M. Kim and K. Kim, *Nature Photon.* **5**, 176 (2011).

[27] H. Huang, A. Dorn, G. P. Nair, V. Bulović, and M. G. Bawendi, *Nano Lett.* **7**, 3781 (2007).

[28] Y. Li, A. Rizzo, R. Cingolani, and G. Gigli, *Adv. Mater.* **18**, 2545 (2006).

[29] H. M. Haverinen, R. A. Myllyla, and G. E. Jabbour, *Appl. Phys. Lett.* **94**, 073108 (2009).

[30] A. Facchetti and T. J. Marks (eds), *Transparent Electronics: From Synthesis to Applications*, (Wiley, Chichester, 2010).

[31] P. P. Edwards, A. Porch, M. O. Jones, D. V. Morgan, and R. M. Perks *Dalton Trans.*, 2995 (2004).

[32] V. Bulović, G. Gu, P. E. Burrows, S. R. Forrest and M. E. Thompson, *Nature* **380**, 29 (1996).

[33] P. E. Burrows, G. Gu, V. Bulović, Z. Shen, S. R. Forrest and M. E. Thompson, *IEEE Trans. Electron Devices* **44**, 1188 (1997).

[34] D. M. Mattox, *J. Vac. Sci. Technol. A* **7**, 1105 (1989).

[35] A. Kumar and C. Zhou, *ACS Nano* **4**, 11 (2010).

[36] J. Meyer, T. Winkler, S. Hamwi, S. Schmale, H.-H. Johannes, T. Weimann, P. Hinze, W. Kowlasky and T. Riedl, *Adv. Mater.* **20**, 3839 (2008).

[37] P. E. Burrows, G. Gu, S. R. Forrest, E. P. Vicenzi and T. X. Zhou, *J. Appl. Phys.* **87**, 3080 (2000).

[38] S. Chen, L. Deng, J. Xie, L. Peng, L. Xie, Q. Fan and W. Huang, *Adv. Mater.* **22**, 5227 (2010).

[39] M. Thomschke, R. Nitsche, M. Furno and K. Leo, *Appl. Phys. Lett.* **94**, 083303 (2009).

[40] D. Zhang, K. Ryu, X. Liu, E. Polikarpov, J. Ly, M. E. Tompson and C. Zhou, *Nano Lett.* **6**, 1880 (2006).

[41] K. S. Kim, Y. Zhao, H. Jang, S. Y. Lee, J. M. Kim, K. S. Kim, J.-H. Ahn, P. Kim, J.-Y. Choi and B. H. Hong, *Nature* **457**, 706 (2009).

[42] S. Bae, H. Kim, Y. Lee, X. Xu, J.-S. Park, Y. Zheng, J. Balakrishnan, T. Lei, H. R. Kim, Y. I. Song, Y.-J. Kim, K. S. Kim, B. Özyilmaz, J.-H. Ahn, B. H. Hong, S. Iijima, *Nature Nanotech.* **5**, 574 (2010).

[43] R. R. Nair, P. Blake, A. N. Grigorenko, K. S. Novoselov, T. J. Booth, T. Stauber, N. M. R. Peres, A. K. Geim, *Science* **320**, 1308 (2008).

[44] C. G.-Navarro, R. T. Weitz, A. M. Bittner, M. Scolari, Alf Mews, M. Burghard and K. Kern, *Nano Lett.* **7**, 3499 (2007).

[45] J. Wu, H. A. Becerril, Z. Bao, Z. Liu, Y. Chen and P. Peumans, *Appl. Phys. Lett.* **92**, 263302 (2008).

[46] J. Wu, M. Agrawal, H. A. Becerril, Z. Bao, Z. Liu, Y. Chen and P. Peumans, *ACS Nano* **4**, 43 (2009).

[47] The synthesis of quantum dots and ZnO nanoparticles used in this thesis was conducted by *Jaehoon Lim*, *Dr. Wan Ki Bae*, *Prof. Seonghoon Lee* and *Prof. Kookheon Char* in Seoul National University.

[48] W. K. Bae, K. Char, H. Hur and S. Lee, *Chem. Mater.* **20**, 531 (2008).

[49] W. K. Bae, M. K. Nam, K. Char and S. Lee, *Chem. Mater.* **20**, 5307 (2008).

[50] J. Lim, S. Jun, E. Jang, H. Baik, H. Kim and J. Cho, *Adv. Mater.* **19**, 1927 (2007).

[51] C. Pacholski, A. Kornowski, and H. Weller, *Angew. Chem., Int. Ed.* **41**, 1188 (2002).

[52] The synthesis of graphene films on plastic substrates used in this thesis was conducted by *Dr. Sukang Bae* and *Prof. Byeong Hee Hong* in Seoul National University.

[53] S.R. Forrest, D.D.C. Bradley and M.E. Thompson, *Adv. Mater.* **15**, 1043 (2003).

[54] S. Wu, *J. Adhes.* **5**, 17 (1973).

[55] T. Young, *Phil. Trans. R. Soc. Lond.* **95**, 65 (1805).

[56] D. K. Owens and R. C. Wendt, *J. Appl. Polym. Sci.* **13**, 1741 (1969).

[57] Z. Wang, J. Zhang, R. Xing, J. Yuan, D. Yan and Y. Han, *J. Am. Chem. Soc.* **125**, 15278 (2003).

[58] A. F. Stalder, T. Melchior, M. Müller, D. Sage, T. Blu, M. Unser, *Colloid Surf. A-Physicochem. Eng. Asp.* **364**, 72 (2010).

[59] V. Wood, M. J. Panzer, J. Chen, M. S. Bradley, J. E. Halpert, M. G. Bawendi and V. Bulović, *Adv. Mater.* **21**, 2151 (2009).

[60] H. Lee, I. Park, J. Kwak, D. Y. Yoon and C. Lee, *Appl. Phys. Lett.* **96**, 153306 (2010).

[61] J. Hou, J. Wu, Z. Xie and L. Wang, *Org. Electron.* **9**, 959 (2008).

[62] G. Williams and P. V. Kamat, *Langmuir* **25**, 13869 (2009).

[63] A. C. Ferrari, J. C. Meyer, V. Scardaci, C. Casiraghi, M. Lazzeri, F. Mauri, S. Piscanec, D. Jiang, K. S. Novoselov, S. Roth and A. K. Geim, *Phys. Rev. Lett.* **97**, 187401 (2006).

Publication

[1] International Journals

1. J. W. Kim, J. W. Jeong, **H. Cho**, C. Lee, Y. T. Hong, S. J. Park, S. K. Kwon, “All-solution-processed bottom-gate organic thin-film transistor with improved subthreshold behavior using functionalized pentacene active layer”, *J. Phys. D-Appl. Phys.* **42**, 115107 (2009).
2. S. H. Kim, **H. Cho**, Y. T. Hong, C. Lee, “Effect of Electrode Area on High Speed Characteristics over 1 MHz of Poly(3-hexylthiophene-2,5-diyl) Diode with Inkjet-Printed Ag Electrode”, *Mol. Cryst. Liquid Cryst.* **513**, 256 (2009).
3. **H. Cho**, S. H. Kim, Y. T. Hong, C. Lee, “Characteristics of Inverters Using Pentacene Organic Thin Film Transistors with Printed Ag Electrodes”, *Mol. Cryst. Liquid Cryst.* **513**, 262 (2009).
4. **H. Cho**, C. H. Jung, M. J. Park, H. K. Shim, D. H. Hwang, C. Lee, “Organic Thin Film Transistors Using a POSS-based Photo-patternable Insulating Material”, *J. Nanosci. Nanotechnol.* **9**, 6923 (2009).
5. **H. Cho**, H. Yoon, K. Char, Y. Hong, C. Lee, “Organic Thin-Film Transistors with Transfer-Printed Au Electrodes on Flexible Substrates”, *Jpn. J. Appl. Phys.* **49**, 05EB08 (2010).

6. C.-H. Jung, **H. Cho**, S.-Y. Lee, Y. Hong, C. Lee, D.-H. Hwang, “Photo-curable epoxy functionalized cyclotetrasiloxane as a gate dielectric for organic thin film transistors”, *Curr. Appl. Phys.* **10**, 1132 (2010).
7. L. Wang, **H. Cho**, S.-H. Lee, C. Lee, K.-U. Jeong, M.-H. Lee, “Liquid crystalline mesophases based on symmetric tetrathiafulvalene derivatives”, *J. Mater. Chem.* **21**, 60 (2011).
8. C.-m. Kang, **H. Cho**, H. Lee, C. Lee, “Organic Rectifier with Transfer-printed Metal as a Top Electrode”, *J. Kor. Phys. Soc.* **59**, 470 (2011).
9. J. Y. Kim, **H. Cho**, S. Noh, Y. Lee, Y. M. Nam, C. Lee, W. H. Jo, “Charge transport in amorphous low bandgap conjugated polymer/fullerene films”, *J. Appl. Phys.* **111**, 043710 (2012)
10. J. Kwak, W. K. Bae, D. Lee, I. Park, J. Lim, M. Park, **H. Cho**, H. Woo, D. Yoon, K. Char, S. Lee, C. Lee, "Bright and efficient full-color colloidal quantum dot light-emitting diodes using an inverted device structure", *Nano Lett.* **12**, 2362 (2012).

[2] International Conferences

1. C. Lee, H. I. Baek, J. H. Kwak, **H. Cho**, “Investigation of degradation mechanisms of oragnic light-emitting diodes under an electrical stress”, Proceedings of International Display Manufacturing Conference, pp.446-448, Taipei, Taiwan (2007).
2. H. I. Baek, **H. Cho**, C. Lee, “Multilayer white organic light emitting diode with optimum emitting layer sequence, Proceedings of the 7th Pacific Rim Conference on Lasers and Electro-Optics”, pp.756-757 (2007).
3. J. Kwak, **H. Cho**, Y. Hong, C. Lee, Effect of Ambient Gas on the Early Stage of the OLED Degradation, Proceedings of the 7th International Meeting on Information Display, pp.1042-1045, Aug 28-31 (2007).
4. C. Lee, **H. Cho**, S. Kim, “Printing technology for high speed printed electronic devices”, 1st International Conference on R2R Printed Electronics (2008).
5. **H. Cho**, S. Kim, Y. Hong, C. Lee, “Characteristics of inverters using pentacene organic thin film transistors with printed Ag electrodes”, The 12th International Symposium on Advanced Display Materials & Devices (2008).
6. S. Kim, **H. Cho**, Y. Hong, C. Lee, “Effect of Area Size on High Speed Characteristics over 1 MHz of Poly(3-hexylthiophene)-2,5-

diyl Diode with Inkjet Printed Ag Electrode", The 12th International Symposium on Advanced Display Materials & Devices (2008).

7. C. K. Suman, J. J. Yang, **H. Cho**, C. Lee, "Studies on conduction mechanism of metal oxide doped organic semiconductor using impedance spectroscopy", ICEL-7, p. 49, Dresden, Germany (2008).
8. **H. Cho**, J. Kwak, C. Lee, "The effect of ambient gas pressure in organic thin film transistors", The 7th International Conference on Electroluminescence of Molecular Materials and Related Phenomena, p. 182, Dresden, Germany (2008).
9. C. H. Jung, J. Kang, **H. Cho**, C. Lee, D. H. Hwang, "Photo-Curable Organic/Inorganic Hybrid Material as an Insulator for Organic Thin Film Transistors", 1st International Symposium on Hybrid Materials and Processing, Grand Hotel Busan, Haeundae, Busan, Korea (2008).
10. C. Lee, S. U. Noh, J. Y. Kim, S. H. Kim, **H. Cho**, "Analysis of the cell area scaling effect on the photovoltaic properties of P3HT:PCBM solar cells", Materials Research Society 2008 Fall Meeting, Boston, USA (2008).
11. J. J. Yang, **H. Cho**, S. U. Noh, Y. T. Hong, C. Lee, "Investigation of temperature dependence of the hole mobility in poly(3-hexylthiophene) thin film transistor", Materials Research Society 2008 Fall Meeting, Boston, USA (2008).
12. **H. Cho**, M. J. Lee, H. S. Yoon, K. H. Char, Y. S. Kim, C. Lee, "Organic thin-film transistors and transistor diodes with transfer-printed Au electrodes", IMID, p.191, Kintex, Korea (2009).

13. **H. Cho**, H. S. Yoon, K. H. Char, Y. T. Hong, C. Lee, “Organic thin film transistors with transfer-printed Au electrodes on flexible substrates”, International Conference on Flexible and Printed Electronics, Jeju, Korea (2009).
14. C. H. Jung, **H. Cho**, C. Lee, D. H. Hwang, “Photo-patternable insulating material for organic thin film transistors”, International Workshop on Flexible & Printable Electronics (2009).
15. C. Lee, C. M. Kang, **H. Cho**, “High-frequency rectifier based on printed organic diodes”, International Workshop on Flexible & Printable Electronics (2009).
16. C.-m. Kang, **H. Cho**, M. Kim, M.-j. Park, Y. Hong, K.-W. Whang, B. H. Cho, C. Lee, “High Frequency Operating Pentacene Rectifying Diode with Inkjet Printed Electrode”, 3rd International Symposium on Flexible Organic Electronics (IS-FOE10), p. 114, Ouranoupolis, Greece (2010).
17. **H. Cho**, M. Kim, M.-j. Park, C.-m. Kang, Y. Hong, K.-W. Whang, B. H. Cho, C. Lee, “Organic Thin Film Transistors Using Transfer-Printed Ag Electrodes”, 3rd International Symposium on Flexible Organic Electronics (IS-FOE10), p. 102, Ouranoupolis, Greece (2010).
18. M. Kim, **H. Cho**, M. Park, C. Lee, “The effect of HMDS treatment on the surface of OTFT dielectric layer for inkjet printing”, International Conference on Science and Technology of Synthetic Metals 2010, 8P-172, Kyoto, Japan (2010).

19. M. Kim, **H. Cho**, J. Kwak, C. H. Lee, “Flexible Ring Oscillator Made of 5-Stage Complementary Organic Inverters”, International Workshop on Flexible & Printable Electronics, P89, Muju, Jeollabuk-do, Korea (2010).
20. M.-j. Park, **H. Cho**, M. Kim, C.-m. Kang, C. Lee, “The Effects of Alkyl SAM Chain Length on Pentacene Thin-Film Transistors”, International Meeting on Information Display 2010, p.490, Kintex, Korea (2010).
21. N. Lee, Y. Bae, J. Lee, **H. Cho**, C. Lee, A. Hirohata, L. Fleet, T. Kim, “Electrode Dependent Spin Injection in a Ferromagnet/Organic Semiconductor Heterostructure”, 2010 MRS Fall Meeting, Boston, USA (2010).
22. Y. Bae, N. Lee, J. Lee, **H. Cho**, C. Lee, T. Kim, “Spin-dependent Transport Properties in a Ferromagnet / Organic Semiconductor / Ferromagnet Heterojunction”, 2010 MRS Fall Meeting, Boston, USA (2010).
23. N. Lee, Y. Bae, J. Lee, **H. Cho**, C. Lee, A. Hirohata, L. Fleet, T. Kim, “Magneto-optoelectronic properties of Fe/MgO/CuPC heterostructures”, 55th Annual Conference on Magnetism and Magnetic Materials, Atlanta, USA (2010).
24. **H. Cho**, J. Kwak, S. Noh, C.-m. Kang, Y. Hong, C. Lee, “High-efficiency organic light-emitting transistors with double light-emitting layers”, The 7th International Thin-Film Transistor Conference, Cambridge, UK (2011).

25. C.-m. Kang, **H. Cho**, M. Park, J. Roh, C. Lee, “Effect of Hole Injection Layers in Pentacene Rectifiers”, The 22nd International Conference on Molecular Electronics and Devices, Pohang, Korea, Best Poster Award (2011).
26. **H. Cho**, C. Lee, J. Kwak, D.-M. Shin, W. K. Bae, J. Lim, K. Char, S. Lee, “Full-Color Patterning of Quantum-Dot (QD) LEDs Using QD Transplanting Techniques”, Society for Information Display 2011 International Symposium, Digest of technical papers, vol. 40, pp. 526-528, Los Angeles, USA (2011).
27. M. Park, **H. Cho**, H. Lee, J. Kwak, C. Lee, “Characteristics of Organic Thin-Film Transistors with a Gate Dielectric Deposited with Self-Assembled Monolayer of Various Alkyl Chain Lengths”, Nano Korea 2011, KINTEX, Korea (2011).
28. J. Roh, M. Park, C.-m. Kang, **H. Cho**, C. Lee, “Enhanced Performance of All-Solution-Processed n-type Organic Thin Film Transistor by Employing Self-Assembled Monolayer”, International Meeting on Information Display, KINTEX, Korea (2011).
29. **H. Cho**, J. Lim, M. Park, D. Lee, K. Char, S. Lee, C. Lee, “Full-color patterning of colloidal quantum dots on an organic hole transport layer using the transplanting technique”, The 10th International Conference on Nanoimprint and Nanoprint (NNT2011), pp.280-281, Jeju, Korea (2011).
30. N. J. Lee, Y. J. Bae, T. H. Kim, **H. Cho**, C. Lee, L. Fleet, A. Hirohata, E. Ito, “Energy Level Alignment at Metal/Organic Semiconductor

Interfaces with Artificially Structured Thin Oxide Layers", 2011 MRS Fall Meeting, Hynes Convention Center, Boston, MA H13.2 (2011).

31. Y. J. Bae, N. J. Lee, T. H. Kim, **H. Cho**, C. Lee, L. Fleet, A. Hirohata, J.-S. Kim, "Annealing effect of the Cu-Phthalocyanine thin films grown on the epitaxial MgO/Fe/MgO(100) layers for organic spintronic applications", The 7th International Conference on Advanced Materials and Devices, p. 363 (2011).
32. N. J. Lee, Y. J. Bae, E. Ito, **H. Cho**, C. Lee, T. H. Kim, "The role of MgO thin films for spin injection into organic light emitting devices", The 7th International Conference on Advanced Materials and Devices, p. 374 (2011).

초 록

최근, 높은 색 순도, 색 조절의 용이함, 공정의 단순함 등의 재료적 특성으로 인하여 조명이나 디스플레이 응용에 관련하여 콜로이드성 양자점을 기반으로 하는 발광다이오드에 대한 관심이 증가하여 왔다. 1994 년 Alivisatos 그룹에 의한 최초 발표 이후, 물질 합성, 전기물리학적 분석, 발광 소자 구조 연구 등에 여러 그룹의 연구 노력과 함께 양자점 발광다이오드의 소자 성능은 꾸준히 향상되어 왔다. 하지만 현재의 성숙된 디스플레이 기술들, 예를 들어 유기발광다이오드에 견줄 만한 성능이 되기 위해서, 양자점 발광다이오드의 성능은 더욱 개선될 필요가 있다.

본 논문에서는 우선 연한 접촉 이식공정 방법으로 만들어진 양자점 발광다이오드 소자의 성능을 연구하였다. 연한 접촉 이식공정으로 제작된 양자점 발광다이오드는 기존의 스핀 코팅 공정으로 제작된 양자점 발광다이오드에 견줄 만한 소자 특성을 보였다. 또한 진공증착되는 여러 정공수송층에 양자점 패턴 능력을 살펴보았다. 정공수송물질과 양자점 사이의 접착 특성이 좋을수록, 전사된 양자점 패턴은 더 좋은 특성을 나타내었다. 양자점 이식공정 방법으로 유기 정공수송물질 위에 손상 없이 양자점을 증착할 수 있으므로, 양자점의 밸런스 밴드(valencd band)에 정공을 유리하게 주입할 수 있는 높은 최고준위점유분자궤도(HOMO, Highest occupied

molecular orbital)을 가지는 정공수송층 위에 양자점을 이식하여 높은 효율의 양자점 발광다이오드를 제작할 수 있었다.

나아가 아연산화물 나노입자를 전자주입층으로 사용하고 인듐주석산화물(ITO, Indium tin oxide) 전극을 음극으로 사용하는 역구조에 p-도핑한 그래핀 전극을 박막 붙임하여 매우 투명하고 유연한 양자점 발광다이오드를 개발하였다. 적 · 녹 · 청 투명유연 양자점 발광다이오드는 뛰어난 투명도와 높은 효율을 보여주었다. 그래핀 전극의 더 높은 투명도로 인해, 청색–녹색 파장 영역에서 그래핀 쪽의 발광이 더 크게 나타났다. 각도에 따른 전기발광 특성이 거의 램버시안(Lambertian) 특성을 따랐다. 마지막으로 인듐주석산화물 전극을 자외선-오존(UV-ozone) 처리된 그래핀 전극으로 대체한 음극과 그래핀 양극으로 사용하는 적 · 녹 · 청 투명유연 양자점 발광다이오드를 성공적으로 개발하였다. 본 논문에서 개발된 공정 방법들과 소자 구조들은 미래의 투명하고 유연한 여러 가지 광전기적 소자들을 실현하는데 유용하게 사용될 수 있을 것으로 생각된다.

주요어: 콜로이드성 양자점, 발광다이오드, 그래핀 전극, 양자점 이식 공정

학 번: 2006-23202

감사의 글

2006 년 9 월부터 시작했던 대학원 생활이 2012 년 8 월 학위를 취득하게 됨으로써 마무리 되어가고 있습니다. 군대도 다녀와서 무엇이든 잘 할 수 있을 거라고 어린 생각을 가졌던 저에게 석박사통합과정 6 년은 지금까지의 삶 속에서 큰 도전이었고 나중의 삶에도 큰 의미가 될 것입니다. 짧지만 감사의 글을 통해서 혼자서는 감당할 수 없었던 이 대학원 생활에 큰 도움을 주신 분들에게 감사의 뜻을 전하고 싶습니다.

우선, 늘 나와 함께 하시고 내 기도에 응답해 주신 아버지 하나님께 감사를 드립니다. 그리고 부족한 저를 항상 아낌없이 지도해 주시고 성장하기까지 계속 관심 가져 주시고 조언해주신 이창희 교수님께 진심으로 감사를 드립니다. 졸업심사에 힘써주시고 졸업논문을 지도해주신 홍용택 교수님, 김연상 교수님, 홍병희 교수님, 곽정훈 교수님께 감사 드립니다. 특별히 졸업 논문을 쓰는데 있어 패터닝 기술들에 많은 조언을 해주신 김연상 교수님과 윤현식 교수님께 감사 드립니다. 양자점 연구에 도움을 주신 차국헌 교수님, 이성훈 교수님, 곽정훈 교수님과 배완기 박사님, 임재훈 씨께 감사 드립니다. 그래핀 전극을 제공해 주시고 조언해 주신 홍병희 교수님과 배수강 박사님께도 감사 드립니다.

한 연구실 안에서 많은 것을 함께했던 선후배들을 또한 잊지 못할 것입니다. 바로 위에 선배로서 많은 것을 가르쳐 준 승욱이와 정훈이(지금은 곽정훈 교수님이 되셨네요) 너무나 고마워요. 신앙 안에서는 형제로 또 연구실 안에서는 가까운 후배로 하지만 이 연구실에 들어오게 되는데 큰 도움을 주었던 정진이 여러 가지로 고맙다. 석사로 마치고 회사에 들어간 진영이 환석이도 고맙고,

지금은 정훈이랑 결혼하고 잘 지내는 지영 누나 고마워요. 또 여러 가지로 조언해 주고 힘주셨던 흠일이 형, 입학 동기 정호 형, 또 원준이형 고맙습니다. 필수 형과 박정호 박사님도 감사합니다. 열심히 또 조용히 실험하느라 많은 얘기를 함께하지 못해 아쉬웠던 치환이형도 감사해요. 늘 크게 웃었던 시스템 IC 팀 서희 잘 따라주어서 함께 해 주어서 고마웠고, OTFT 하느라 고생했던 민규도 고맙고, 태양전지 용주, 졸업하고 회사간 준엽이, 그리고 동생 같은 혁이도 고맙다. 실험 논의를 잘 해줬던 현구에게 고맙고 같이 OLED 파트에서 중요한 역할을 감당할 용원에게도 고맙고, 항상 믿음직한 동생으로 또 형으로서 날 잘 대해줬던 찬모와 동구 또한 준영에게 고맙고, 방장으로 수고하는 명진이에게도 고맙고 앞으로도 잘 해나가길 기도할께. OTFT 를 맡아 정말 잘 하고 있는 정균이 앞으로도 현우와 같이 연구 잘하기를 바라고, 내 일을 많이 물려 받게 된 희영이도 지금 하듯이 차근차근 연구 잘 해나가기를 기도할께. 태양전지 멤버로 새로 들어온 형준, 지연, 호정, 영준에게도 고맙고 연구 잘하길 바라고, 시스템 IC 초창기부터 함께 했던 설미도 고마워요. 연구실 사람들 모두, 힘들 때 또 기쁠 때 함께 해준 것에 대해 정말 감사 드립니다.

연구실에서 들어와 사귀고 결혼까지 하게 된 내 아내 경하에게 항상 기도로 후원해주고 날 이해해 준 것에 감사하고, 진심으로 응원해주신 부모님과 장인 장모님께 감사 드리고, 또한 동생 현민이 가족과 처남 진형에게도 감사를 드립니다. 마지막으로 다시 한번 항상 함께 해주시는 아버지 하나님께 감사 드리고, 모든 졸업의 영광을 아버지 하나님께 돌려 드립니다.

2012 년 8 월

조 현 덕